The surface area and reactivity of granitic soils: I. Dissolution rates of primary minerals as a function of depth and age deduced from field observations

Samuel A. Parry[a*], Mark E. Hodson[b], Simon. J. Kemp[c], Eric H. Oelkers[d,e]

[a] Soil Research Centre, Dept. Geography and Environmental Science, School of Human and Environmental Sciences, University of Reading, RG6 6DW, UK. s.a.parry@reading.ac.uk

[b] Environment Department, University of York, YO10 5DD, UK, mark.hodson@york.ac.uk

[c] British Geological Survey, Keyworth, Nottingham, NG12 5GG, UK. sjk@bgs.ac.uk.

[d] GET-OMP, Université Paul Sabatier/CNRS-UMR 5563, 31400 Toulouse, France. oelkers@get.obs-mip.fr

[e]Department of Earth Sciences, University College London, Gower Street WC1E 6BT, UK.

[*]Corresponding author. Present address: 8 High Street, Greenhithe, Kent, DA9 9NN, UK. samuelparry84@googlemail.com.

ABSTRACT---

Surface area-normalized dissolution rates of the primary minerals in two distinct granitic soils located in 1) the Dartmoor National Park, England and 2) Glen Dye, Scotland were determined as a function of depth. Each soil was sampled to a depth of ~1 m. The maximum soil ages based on ^{14}C analysis of the humin fraction of the soil are 15,600 and 4,400 years for the Dartmoor and Glen Dye soil profiles, respectively. The measured BET surface areas of the soil minerals are close to 5 m^2/g in the B and C horizons, but decrease to less than 1 m^2/g close to the surface. Retrieved geometric surface area normalized mineral dissolution rates are most rapid at the surface and at the bedrock-soil interface; this behaviour is interpreted to stem from a combination of the approach to equilibrium of the soil waters with depth and more rapid dissolution rates of fresh versus weathered surfaces. At the soil surface, the relative mineral dissolution rate order is found to be quartz > feldspar > mica, with quartz geometric surface area dissolution rates as fast as 2.6 to 4.1 x 10^{-13} $mol/m^2/s$. As observed in a number of past studies, field based rates obtained in this study are significantly slower that

corresponding rates obtained from laboratory studies, suggesting these latter rates may not accurately describe the reactivity of primary minerals in soils.

The surface area and reactivity of granitic soils: I. Dissolution rates of primary minerals as a function of depth and age deduced from field observations

Samuel A. Parry[a*], Mark E. Hodson[b], Simon. J. Kemp[c], Eric H. Oelkers[d,e]

[a] Soil Research Centre, Dept. Geography and Environmental Science, School of Human and Environmental Sciences, University of Reading, RG6 6DW, UK. s.a.parry@reading.ac.uk

[b] Environment Department, University of York, YO10 5DD, UK, mark.hodson@york.ac.uk

[c] British Geological Survey, Keyworth, Nottingham, NG12 5GG, UK. sjk@bgs.ac.uk.

[d] GET-OMP, Université Paul Sabatier/CNRS-UMR 5563, 31400 Toulouse, France. oelkers@get.obs-mip.fr

[e]Department of Earth Sciences, University College London, Gower Street WC1E 6BT, UK.

[*]Corresponding author. Present address: 8 High Street, Greenhithe, Kent, DA9 9NN, UK. samuelparry84@googlemail.com.

ABSTRACT---

Surface area-normalized dissolution rates of the primary minerals in two distinct granitic soils located in 1) the Dartmoor National Park, England and 2) Glen Dye, Scotland were determined as a function of depth. Each soil was sampled to a depth of ~1 m. The maximum soil ages based on ^{14}C analysis of the humin fraction of the soil are 15,600 and 4,400 years for the Dartmoor and Glen Dye soil profiles, respectively. The measured BET surface areas of the soil minerals are close to 5 m^2/g in the B and C horizons, but decrease to less than 1 m^2/g close to the surface. Retrieved geometric surface area normalized mineral dissolution rates are most rapid at the surface and at the bedrock-soil interface; this behaviour is interpreted to stem from a combination of the approach to equilibrium of the soil waters with depth and more rapid dissolution rates of fresh versus weathered surfaces. At the soil surface, the relative mineral dissolution rate order is found to be quartz > feldspar > mica, with quartz geometric surface area dissolution rates as fast as 2.6 to 4.1 x 10^{-13} $mol/m^2/s$. As observed in a number of past studies, field based rates obtained in this study are significantly slower that

corresponding rates obtained from laboratory studies, suggesting these latter rates may not accurately describe the reactivity of primary minerals in soils.

Keywords: Soil weathering, Critical zone, Mineral dissolution kinetics, Soil production rate (SPR)

---

1. Introduction

The relative rates of soil erosion versus soil production are critical to the long-term sustainability of the world's agriculture (Montgomery 2007; Heimsath at al., 2012). Perhaps the most significant processes controlling soil production rates is silicate mineral weathering (e.g. Anderson et al., 2007; Dixon and von Blanckenburg, 2012; Navarre-Sitchler et al., 2013). Moreover, the weathering of silicate rocks, which comprise 90% of Earth's crust, is the ultimate source of most essential plant nutrients including phosphorus and base cations (Hartmann et al., 2014; Sverdrup et al., 2006; Sverdrup and Rosen, 1998). The accurate understanding of such weathering rates is, therefore, essential to predict the life-cycle and nutrient availability of soils (Klaminder et al., 2011). The goal of this study is to further our understanding of the silicate mineral weathering rates in soils. Towards this goal, the mineral content of two distinct granitic soil profiles were measured and used to determine their dissolution rates. The purpose of this manuscript is to report these dissolution rates and use them to assess the applicability of laboratory based rates to describe natural weathering processes.

A large number of past studies have focused on quantifying mineral weathering rates in natural systems (e.g. Clow and Drever, 1996; Drever and Clow, 1995; Maher et al., 2009, Maher, 2010; Oliva et al., 2003; Price and Vebel, 2003; White et al., 2008, 2009). Much of this work has been motivated to illuminate the link between continental weathering rates,

atmospheric CO_2 content, and climate (e.g. Brady, 1991; Brady and Carroll, 1994; Gaillardet et al., 1999; Egli et al., 2003; Gislason et al., 2006, 2009; Kump et al., 2000; Moquet et al., 2011; Rasmussen et al., 2011; Volk, 1987; Walker et al., 1981; White and Blum, 1995). Other studies have been motivated to characterize the chemical evolution of the 'critical zone' (e.g. Anderson et al., 2007; Banwart et al., 2011; Brantley et al., 2011; Braun et al., 2012; Buss et al., 2008; Dere et al., 2013; Ma et al., 2011; Salehikhoo et al., 2013). Essential to characterizing weathering rates in natural systems is a detailed understanding of the dissolution rates of primary minerals. Despite the many studies cited above, only a limited number have generated dissolution rates of primary minerals in natural systems (e.g. Hausrath et al., 2011; Schaller et al, 2010; Sverdrup, 1990; White, 2002; White et al., 1996, 2001; Zhu, 2005; Zhu et al., 2004). This study has been designed to help overcome this knowledge gap by determining the dissolution rates of the major silicate minerals in two distinct granitic soils as a function of depth.

2. Materials and methods

2.1 Site selection and sampling

Granitic podzols were sampled from two uncultivated sites, the first located to the South of Princetown in the Dartmoor National Park (DM02, UK Ordnance survey: SX 622,715; latitude and longitude: N50°31`37`` W3°56`44``, altitude: 378 m), and the second in the Glen Dye catchment in South-East Aberdeenshire (GD02, UK Ordnance survey: NO 651,839; latitude and longitude: N56°56`42`` W2°34`31``, altitude: 280 m) (see Fig. 1). In each case, the sample site was covered with grass and bracken; no trees or shrubs were located in the immediate vicinity of these sites. To constrain soil source to the greatest possible degree, the sample sites are directly underlain by bedrock and situated on upland areas of relatively shallow slopes that limited lateral soil movement.

The Dartmoor site (DM02) site is directly underlain by the Dartmoor granite, a coarse porphyritic biotite granite (Exley and Stone, 1964), that formed about 280 mya (Chesley et al., 1993). The mean monthly temperature of this region ranges from 6 to 16 °C and the mean annual rainfall is ~2.0 m/yr. The Glen Dye site (GD02) site is directly underlain by the Water of Dye granite, a coarse pink granite, rich in K-feldspar (Stutter et al., 2004) that formed about 435-390 mya (Soulsby et al., 2004). The mean monthly temperature of this region ranges from 4 to 13°C and the mean annual rainfall is ~1.4 m/yr.

The two sample sites were chosen because they have similar bedrock mineralogies but different geologic histories. During the last glacial maximum, approximately 22 ka (Bowen et al., 2002), the British and Irish ice sheet covered the Glen Dye catchment, but its maximum southern onshore extent lay on the North Somerset coast, roughly 120km North-East of the Dartmoor sample area (Bowen et al., 2002; see Fig. 1). Therefore, Tertiary and periglacial Quaternary soils in Dartmoor may have been preserved, but in Glen Dye the granitic bedrock would have been scoured clean by glacial activity and/or covered by glacially associated materials.

Bulk soil and rock samples were systematically collected over the full soil profile by excavating a pit and then cutting back into the exposed pit faces and taking composite samples for a given depth range. The bulk soil samples were taken systematically at equidistant depths as composite samples. The DM02 samples were taken at depths of 0 – 13, 13 – 36, 26 – 39, 39 – 52, 65 – 78, and 78 – 91 cm. The GD02 samples were taken at depths of 27 – 36, 36 – 45, 45 – 54, 54 – 63, 63 – 72, and 72 – 81cm; the first 27 cm thickness of this site was a peat horizon that we have discounted due to its negligible mineral content. In the

figures, data points are plotted at the mid–point of these ranges. Soils were sampled over systematically spaced ranges in an attempt to limit the effect of small scale heterogeneities and as such do not correspond directly to the eluviation horizons present between 17-27 and 40-50cm depth in the DM02 and GD02 soil profiles. Rock clasts were taken from the deepest sample depth and are assumed to represent altered bedrock. Bedrock samples were collected from the base of the soil pits at 98 and 82cm depth in the DM02 and GD02 soil profiles respectively, using a hammer and chisel. In the figures below, the altered rock clasts and bedrock are plotted at depths of 95 and 100 cm respectively. The DM02 and GD02 soil profiles are described in further detail in Table 1. Bulk soil and rock samples were stored and transported in clean and sealed plastic buckets and zip-lock plastic bags respectively. Prior to analysis, the bedrock samples were cut using a rock saw and further cleaned with a diamond encrusted drill to isolate volumes of material with no indications of weathering (e.g. iron staining).

Samples for ^{14}C dating were collected from fresh pit faces to reduce the potential sources of contamination. Clean nitrile gloves and plastic utensils were used for each sample. Care was taken to avoid contamination by contemporary carbon sources, such as modern roots. After collection, samples were immediately placed in aluminium foil sheets, which were then folded into packages and placed inside polyethylene zip-lock bags. Samples for ^{14}C dating were stored in the dark at a constant temperature below $4^{o}C$ prior to analysis.

2.2 Characterisation of solids

The chemical and physical properties of the soil were determined. Soil was air-dried at 40 °C to constant mass and sieved to < 2mm. Subsamples were then heated overnight at 105 ºC to determine moisture content and generate correction factors so that concentration

measurements determined on air-dried soil could be expressed on the basis of oven dried soil. The following measurements were then made on < 2mm, air-dried soil. Loss on ignition as a proxy for organic matter content was determined by mass change on triplicate samples following overnight ignition of soil at 500 °C (Rowell, 1994). pH was determined on triplicate samples using a Jenway 3310 pH probe calibrated at pH 7.00 and 4.00 using BDH Laboratory supplies pH buffers (Rowell, 1994). The chemical composition of the soil and rock samples was determined by X-ray fluorescence spectrometry (XRFS). Representative ~ 5g air-dried subsamples were agate milled, pressed into pellets, and then analysed using a Philips PW 1480 X-ray fluorescence spectrometer, with a dual anode Sc/Mo 100kV 3kW X-ray tube, and using Philips X40 analytical software. The standard error (99.7% confidence level) for major elements is typically 5%, and the nominal detection limit of trace elements is 5ppm. The XRFS output was initially expressed as weight percent oxides, these were normalised to 100% and recalculated to concentrations expressed as mol kg^{-1}.

The organic matter present in the < 2mm samples was subsequently removed by sodium hypochlorite (NaOCl) oxidation following the method of Kaiser et al. (2002). 1M aqueous NaOCl was adjusted to pH 8.5 using concentrated HCl and a Jenway 3310 pH probe. The pH probe was calibrated at pH 7.00 and pH 9.22 using BDH Laboratory Supplies pH buffers. Soil samples were placed in acid washed 750ml polypropylene centrifuge bottles with the pH adjusted NaOCl at a ratio of 1:50 by weight for 6 hours at 25°C, and were shaken at 120rpm in an orbital shaking Grant OLS200 water bath. Samples remained in the pH adjusted NaOCl overnight, and were then centrifuged at 1570 g for 15 minutes using a MSE Mistral 3000i centrifuge. The reacted supernatants were removed by Finnpipette; this procedure was repeated 5 times. Following the final oxidation and centrifuging procedure, the solids were washed in ultrapure H_2O seven times or until the supernatants became clear. If SOM was still

visible, the procedure was repeated. Upon completion, the soil samples were washed in ceramic evaporating dishes using ultrapure H_2O, evaporated under infrared lamps, dried at 40°C in a Memmert oven overnight, and then stored in zip-lock bags at room temperature.

Following organic matter removal, mineralogy by X-ray diffraction, particle size distribution by laser granulometry, and BET surface area (A_{BET}) were determined. The mineralogies of the soil and rock samples were investigated using powder X-ray diffraction (XRD) analysis employing a PANalytical X'Pert Pro series diffractometer equipped with a cobalt-target tube and a X'Celerator detector and operated at 45kV and 40mA. Samples were prepared following the methodology outlined by Kemp and Merriman (2009). Micronised powders, spiked with 10% corundum (American Elements - PN:AL-OY-03-P) internal standard were scanned from 4.5-85°2θ at 2.76°2θ/minute. Crystalline phases were identified using PANalytical X'Pert Highscore Plus software coupled to the latest version of the International Centre for Diffraction Data (ICDD) database. The relative proportions of minerals and amorphous material present were assessed using the internal standard Rietveld refinement technique (Madsen and Scarlett, 2008; Snyder and Bish, 1989; Young, 1993) and the PANalytical X'Pert Highscore Plus software. The uncertainty in these compositions is on the order of ±2%. Rietveld analysis inherently produces a sum of phases normalised to 100%. For accurate analysis, all the phases must be identified and their crystal structures known. If amorphous or unknown phases are present, the proportions of the crystalline phases will be overestimated. This problem was overcome by the addition of the corundum reference standard, as described above. The proportion of crystalline phases present was calculated by first determining the ratio between the corundum concentration determined by Rietveld analysis and its true value. The percent of amorphous (or unknown) phases is given by subtracting 1 from this ratio then multiplying this difference by 100.

Particle size distribution was determined using a combination of dry sieving and a Beckman Coulter LS230 laser granulometer. Approximately 5 g of sample was sieved to 1 mm; both fractions were weighed. The < 1 mm fraction was dispersed in aqueous sodium hexametaphosphate and its particle size distribution determined using laser granulometetry and the Fraunhofer optical model (de Boer et al., 1987). The mass of the > 1 mm fraction and the laser granulometer output were combined to calculate the sample fraction present in the size ranges < 2 μm (clay), 2 – 63 μm (slit), 63 – 250 μm (fine sand), 250 – 500 μm (medium sand) and 500 – 2000 μm (coarse sand).

The particle size distribution data were used to calculate geometric surface areas for each size fraction assuming that the particles were smooth spheres with a density of 2.56 g cm^{-3} using

$$A_{GEOM,i} = 6 / \rho \, . \, d_{e,i} \quad (1)$$

where $A_{GEOM,i}$ refers to the geometric surface area of the i*th* fraction (m^2 g^{-1}); ρ stands for the density of the solid (g cm^{-3}) and; $d_{e,i}$ represents the effective spherical diameter of the i*th* fraction (μm) which can be computed using (Gautier et al., 2001)

$$d_{e,i} = (d_{max,i}-d_{min,i}) / \ln(d_{max.i}/d_{min,i}) \quad (2)$$

where $d_{max,i}$ and $d_{min,i}$ signifies the maximum and minimum particle diameter of the i*th* fraction (μm) (Tester et al., 1994)

The $A_{GEOM,i}$ were then combined to generate a total geometric surface area A_{GEOM} for the < 2mm bulk soil using

$$A_{GEOM} = \Sigma\, x_i \,.\, A_{GEOM,i}/100 \quad (3)$$

where x_i refers to the mass percentage of the i*th* fraction in whole sample

2.3 Mass transfer modeling

Minerals lost or gained during weathering in the soil profiles were calculated using the mass transfer co-efficient τ (White, 2002). When τ = -1 total depletion of the mineral has occurred, and if $\tau > 0$ enrichment of the mineral has occurred. τ is calculated from the ratio of the compaction corrected mass of a mineral in a soil profile relative to that of the parent rock ($\tau_{i,d}$)

$$\tau_{i,d} = \left(m_{i,d,corr} / m_{i,bedrock}\right) - 1 \quad (4)$$

where $m_{i,d,corr}$ refers to the mass of the i*th* mineral in each kg of soil at a depth of d after its correction for rock compaction due to material loss and $m_{i,bedrock}$ refers to the mass of the i*th* mineral in each kg of the bedrock.

$m_{i,d,corr}$ is calculated from $m_{i,d,}$ the mass of the i*th* mineral present in each kg of soil at depth d before its correction for rock compaction (i.e. using the bulk soil XRD mineralogy determined at a particular depth) and a correction factor F_d using

$$m_{i,d,corr} = m_{i,d} / F_d \quad (5)$$

The correction factor, F_d, is calculated from:

$$F_d = \frac{c_{Ti,d}}{c_{Ti,bedrock}} \quad (6)$$

where $c_{Ti,d}$ and $c_{Ti,bedrock}$ designate the Ti concentration in the soil sample at depth d in the soil and in the corresponding bedrock, respectively.

Calculations assume that the soil was only derived from the bedrock and Ti is an immobile element, such that it can be used to account for the concentration and dilution effects caused by gains and losses of all the other components (White, 2002). This approach also assumes that Ti input to the soils due to such processes as aeolian dust deposition (e.g. Reheis 1990) is negligible.

2.4 Radiocarbon dating

The dating of soils is a pre-requisite to determining field weathering rates. A variety of different techniques have been used to constrain soil ages. As an estimate of a maximum age, soils in glaciated terraines in which previously developed soils were stripped away by glacial ice to expose fresh bedrock can be assumed to be the same age as the end of the last glaciation. The use of cosmogenic isotopes for dating is becoming more common (Dixon et al., 2009; Heimsath et al., 2012; Norton and von Blanckenburg, 2010; Riggins et al., 2011), and U-Th dating has potential though has not been widely adopted (Dequincey et al., 1999; Maher et al., 2004; Sharp et al., 2003). ^{14}C dating has also been used to date soils (e.g. Chen et al., 2013; Dreibrodt et al., 2013; Favilli et al., 2009; Hiruma et al., 2013; Matthews and

Dresser, 1983; Pressenda et al., 2001; Ricker et al., 2012; Tonneijck et al., 2006; Wakabayshi et al., 2012; Zollinger et al., 2013). All of these methods rely on assumptions that render any derived age to be somewhat uncertain. For example, factors that may alter the ^{14}C dating of soils include 1) a significant time lag before organic matter begins to accumulate in the soil after it is formed, and 2) a downward movement of soil carbon either in solution or via cryo- or bio- turbation (e.g. Scharpenseel, and Becker-Heidmann, 1992; Wang et al., 1996). To limit some of these potential ambiguities, attempts have been made to analyze immobile carbon fractions, for example the humin fraction of soil (c.f. Pressenda et al., 2001).

Soil ages in the present study were estimated from the ^{14}C ages of the humin fraction of sampled soils. This approach is justified in part because our soils showed no indication of cryo- or bio-turbation. ^{14}C dating was carried out using the NERC Radiocarbon Facility. The limitations of this method has been discussed previously in the literature (e.g. Martin and Johnson, 1995; Scharpenseel, and Becker-Heidmann, 1992). Notably, measured ^{14}C ages tend to be younger than the true ages of the soils due to continuous input of organic material into soils (Wang et al., 1996). Samples were first digested in 2M HCl at 80° C for 8 hours, then rinsed with deionised water and digested in 1M KOH at 80° C for 2 hours. The digestion was repeated until no further humics were extracted. The residue was rinsed, digested in 1M HCl at 80° C for 2 hours then rinsed free of acid, dried, and homogenised. Following drying and homogenizing, samples were combusted to CO_2 either in a high-pressure bomb (in the presence of high purity oxygen) (Harkness and Wilson, 1972) or, for smaller samples, in sealed quartz tubes (Boutton et al., 1983). CO_2 was cryogenically separated from other combustion products. CO_2 was converted to an iron-graphite mix using iron/zinc reduction (Slota et al., 1987). ^{14}C analysis by accelerator mass spectrometry was performed at the Scottish Universities Environmental Research Centre (SUERC) using the 0.25MV Single

Stage Accelerator (Freeman et al., 2010). The ^{14}C enrichment of each sample was measured as a percentage of the ^{14}C activity relative to a modern standard (oxalic acid provided by the US National Bureau of Standards, now National Institute of Standards & Technology), where 100% modern is defined as the value in AD 1950, in the absence of any anthropogenic influences (Stuiver and Polach, 1977). Stable carbon isotope ratios were measured on CO_2 sub-samples using a dual-inlet mass spectrometer with a multiple ion beam collection facility (VG OPTIMA) to normalise ^{14}C data to –25 ‰ $\delta^{13}C_{VPDB}$.

3. Results

3.1 Soil characteristics

Measured BET and calculated geometric surface areas after organic material removal from the solids collected from DM02 and GD02 are shown in Fig. 2 (see also Supplementary material Tables S1 and S2). The BET surface areas for the DM02 profile remain relatively constant at ~6 m^2/g at depths below 30 cm, then decrease substantially to less than 1 m^2/g at shallower depths in the Ae and O horizons. A similar variation with depth is found for the GD02 profile. The measured BET surface areas of the GD02 profile are near constant at ~4 m^2/g at depths greater than 55 cm but decrease to 1 m^2/g or less at shallower depths in the Ae and O horizons. The BET surface area increase at ~30 and ~55 cm in depth in these soils occurs when passing from the A to B horizons (see Table 1), where a significant increase in iron is observed. As such this surface area increase likely stems from the presence of iron (oxy)hydroxide minerals. The geometric surface areas are far lower than their BET counterparts, suggesting a significant roughness of the soil grains. A_{GEOM} for the DM02 soils range from 0.09 to 0.38 m^2/g whereas the A_{GEOM} for the GD02 soils range from 0.20 to 0.48 m^2/g

The measured variation of soil organic material content and pH at the two field sites is illustrated in Fig. 3. The upper half of the both soil profiles contain high organic matter contents reflecting the peaty nature of the soil; the soils contain <~4% organic matter at depths greater than 40 cm. The soil pH is particularly low in the upper horizons due to the peaty nature of the soil, but increases down profile.

The measured elemental composition of the soils is shown as a function of depth in Fig. 4. The soils contain similar amounts of Si, Al, and K but significantly less Na and Ca than the original bedrock suggesting significant loss of Na- and Ca- bearing phases during weathering. Mg and Fe are enriched in the soils relative to the bedrock suggesting their association with weathering products. The distinct minima in Fe concentration at ~20 cm in DM02 and 40 cm in GD02 correspond to the presence of an eluviation horizon.

The measured Ti concentrations with depth are illustrated in Fig. 5. The altered bedrock contains significantly more Ti than the bedrock, but has similar concentrations to the soil in DM02. In contrast, the altered bedrock in GD02 has a Ti concentration that is closer to the bedrock. This may indicate significantly more weathering in the DM02 altered bedrock sample. Ti increases up through the soil profiles as would be expected for an immobile element. Thus, although several studies have noted that Ti can be somewhat mobile in soils (e.g. Hodson, 2002; Kurtz et al., 2000; Swindale and Jackson, 1956; Viers et al., 2000) in this study we adopted the practical assumption that Ti is immobile (e.g. Gislason et al., 1996; White, 2009; White et al., 1996). Note that even if Ti is mobile, it is far less mobile than the major elements present in silicate minerals (Hodson, 2002), so that its slight mobility adds only minor uncertainty to the weathering rate calculations presented in this study.

The bulk soil mineralogy is plotted against depth for the two profiles in Fig. 6 (see also Supplementary material Tables S1 and S2). For both profiles the altered bedrock contains less plagioclase and muscovite but slightly more K-feldspar than the fresh bedrock. The altered bedrock in DM02 also contains more chlorite than the original bedrock. Concentrations of plagioclase, K-feldspar, and muscovite then decrease up the soil profile with marked decreases in the upper half of the profile. The feldspar trends mirror those of the Ca, K, and Na trends illustrated in Fig. 4. Despite the decreasing concentrations up profile, the muscovite concentrations are greater than those in the bedrock. Quartz concentrations increase from the bedrock up through the profile but, like the feldspar concentrations show a substantial decrease in the upper most horizon. Inorganic amorphous material, most likely Fe-Al-Si oxyhydroxides was detected in the upper soil horizon of both profiles and, for DM02, at greater depth though in lesser concentrations. Low (< 0.5 wt %) concentrations of chlorite, haematite, and kaolinite were detected in both profiles. Despite weathering, relatively few secondary minerals were detected. A separate XRD analysis of the < 2 μm fraction (not reported here) detected illite, kaolinite, chlorite and smectite in both soils together with hydrobiotite in DM02 and vermiculite in GDO2; illite and kaolinite were the dominant minerals in this fraction. The low mass of clay-sized particles in the soil prevented some of these minerals from being detected in the bulk mineral fraction XRD. The relatively low concentration of secondary minerals could be due to the low pH of the soils (see Fig. 3), keeping solutions undersaturated with respect to secondary weathering products. It is also possible that, due to the high rainfall in the two areas, as dissolution proceeds, cations were washed out of the soil rather than remaining in the pore waters.

3.2 Mass transfer modeling

356 The elemental and mineralogical trends in the soil profiles are influenced by gains and losses
357 of specific elements, as well as physical impacts on the profile such as compaction or volume
358 increases. Therefore τ-values for the elements and minerals were calculated (White, 2009);
359 the results of these calculations are shown in Figs. 7 and 8. These plots show that a significant
360 loss of elements (particularly for profile DM02) and minerals (particularly plagioclase but
361 also muscovite), occurs during bedrock weathering even prior to soil formation. All the soil
362 horizons are significantly depleted in quartz and the feldspars relative to the bedrock and this
363 loss is mirrored by the loss of Na, Ca, and K. In the DM02 profile the positive tau values of
364 Fe suggest that it is incorporated into weathering products. In the GD02 profile, no chlorite
365 was detected in the soil horizons but Fe is less depleted than elements associated with the
366 major silicate phases present. The only Mg-bearing phase detected in our samples by X-ray
367 diffraction was chlorite but the tau values for Mg and chlorite do not show the good
368 agreement observed for K with K-feldspar and Na with plagioclase. In particular, in the GD02
369 profile there is an enrichment in Mg in the lower part of the profile despite the absence of
370 detectable chlorite in the soil samples (trace chlorite was present in the bedrock and altered
371 bedrock samples generating the tau value for chlorite in the altered bedrock in Fig. 8b). The
372 mismatch in the chlorite and Mg tau values in the DM02 profile is possibly due to variations
373 observed in the chemical composition of chlorite (Deer et al., 2013), whilst in the GD02
374 profile there must be an alternative, possibly amorphous, Mg-bearing phase. The tau values
375 for muscovite indicate its loss up profile. For the DM02 profile, there is an increase in
376 muscovite relative to the parent material in the lower horizons. This may indicate that the
377 muscovite concentration of the parent material was unrepresentative since the negative tau
378 values for muscovite up profile are indicative of mineral weathering, or may correspond to
379 muscovite growth related to the observed dissolution of feldspar. No muscovite was detected
380 in the < 2 μm fraction that was analysed by X-ray diffraction, so it seems unlikely that this

enrichment in the lower horizons is due to fine-grained muscovite being carried down the profile by percolating rainwater.

3.3 Radiocarbon dating

The variation of the soil humin fraction conventional radiocarbon age with sample depth is illustrated in Fig. 9 (see also Supplementary material Tables S1 and S2). The soil humin ages were most recent at the surface of both profiles and increased downwards. This suggests that the majority of SOM was input at the soil surface. The SOM becomes older as more material accumulates above it and the soil-bedrock interface moves downwards. The slight decrease in the age of the soil humin fraction at the base of the DM02 soil profile may be due to contamination during sample collection. The maximum soil age measured for the DM02 and GD02 soils was 15,600 and 4,400 years, respectively. These maximum ages compare reasonably with those reported for similar soils in these regions giving us confidence in the results despite the uncertainties associated with soil ^{14}C dating (see above). For example, the ages of soil profiles located on a Bodmin Moor, UK hilltop, located ~50 km west of the DM02 site, measured by ^{10}Be concentrations in rock at the soil interface ranged from 15,000 to 83,000 years (Riggins et al., 2011). Equally, the ages of six soil profiles of the Glen Feshie, located ~80 km west of the GD02 site, measured by carbon dating range from 80 to 13,000 years in age (Bain et al., 1993; Hodson et al., 1998) and the last glaciation in Scotland is estimated to have ended c. 13 ka BP. The differences in these soil ages highlights the difficulty of constraining soil age, and is consistent with the commonly reported observation the organic carbon ^{14}C ages tend to be somewhat lower than the soil itself. Based on these differences, we estimate that uncertainty in soil age contributes an uncertainty of a factor of three to five in our calculated soil ages, and thus the mineral dissolution rates reported below.

406 *3.4 Mineral weathering rates*

407 The approach adopted in the present study to generate primary silicate dissolution rates from
408 soil profiles follows that of White et al. (2002). In this approach, mineral dissolution rates are
409 determined from their mass loss as a function of depth in a single soil. This method avoids
410 computational and interpretative ambiguities that might arise due to differing bedrock
411 compositions and/or hydrologies if rates were generated by comparing mineral mass loss from
412 samples collected from distinct localities. Moreover, this approach allows estimates of silicate
413 mineral dissolution rates as a function of soil depth, a critical factor in modelling soil
414 evolution.

415

416 Silicate mineral dissolution rates expressed as moles of mineral dissolved per unit area per
417 unit time for samples from different depths were determined using

418

$$r_i = \frac{1}{M_i} \frac{\left(\frac{\Delta m_{i,corr}}{\Delta x}\right)\left(\frac{\Delta x}{\Delta a}\right)}{\left(\frac{m_i}{\sum_i m_i} A_{soil}\right)} \quad (7)$$

419

420 where M_i refers to the molecular weight of the *i*th mineral. The two upper parenthetical terms
421 in Eqn. (7) determine 1) the mass loss of the *i*th mineral from the soil ($\Delta m_{i,corr}$) relative to the
422 bedrock divided by the distance between the sample and the soil – bedrock interface (Δx) and
423 2) the change in soil depth with time obtained from the slope of a plot of soil ^{14}C age against
424 depth shown in Fig. 9. The bottom parenthetical term gives the surface area of the *i*th mineral
425 available for dissolution calculated as the weight percent of the *i*th mineral in the soil
426 multiplied by the surface area of the soil sample (see below). It should be emphasized that the
427 approach adopted in this study as quantified using Eq. (7) allows determination of the
428 dissolution rates of all those minerals in the soil profile as long as their masses and surface
429 areas are known as a function of depth.

The choice of whether to use geometric or BET surface area in such equations is the matter of debate in the literature (e.g. Gautier et al., 2001; Hodson, 2006; Köhler et al., 2005; Lee et al., 1998; Stillings and Brantley, 1995; Turpault and Trotignon, 1994) and consequently we solved Eqn. (7) using both terms. A further challenge with ascribing surface area values to determine mineral weathering rates in the field is the partitioning of bulk surface area to the different mineral components. It is rarely practical or possible to separate out the individual mineral species and determine the surface area of each component. Here we have assumed that the surface area of each mineral in the soil is proportional to its weight fraction in the soil. This assumption will be valid for geometric surface area calculations if each mineral has similar size distributions. With the exception of the < 2 μm fraction (which makes a relatively small contribution to total surface area due to the low wt% of < 2 μm sized particles in the soil) this has been shown to be approximately the case for these soils (Parry, 2012). This assumption is harder to justify for BET surface area as secondary minerals can have elevated BET surface areas and distinct surface roughness (e.g. Hodson et al., 1998; Lee et al. 1998). Nonetheless although this pragmatic assumption imparts some uncertainly in the calculations, it has been shown to provide a reasonable first estimate of whole rock reactivity (c.f. Gudbrandsson et al., 2011).

Mineral dissolution rates determined from Eqn. (7) together with the mineralogy reported in Fig. 6 and the soil ages depicted in Fig. 9 are shown in Fig. 10 and 11 (see also Supplementary material Tables S3 and S4). Rates normalised to geometric surface area are greater than those normalised to BET surface area as the surface area term appears as a denominator in Eqn. (7) and values of geometric surface area are significantly lower than

454 BET values (Fig. 2). However, regardless of the surface area term used, the calculations
455 indicate that dissolution rates are greatest at the top and bottom of the soil profile.
456
457 The calculated silicate mineral dissolution rates are very similar between the two profiles with
458 only the potassium feldspar rates being significantly different (Mann Whitney test, $p \leq 0.001$).
459 Levels of rainfall and temperature are greater at the Dartmoor site which should increase
460 weathering rates (White and Blum, 1995), however, the Dartmoor profile is older than the
461 Glen Dye profile, suggesting that rates might be expected to be higher for the Glen Dye
462 profile (e.g. Hodson and Langan, 1999; White et al., 1996). It appears that these antagonistic
463 factors have cancelled each other out to the first approximation.
464
465 **4. Discussion**
466 *4.1 Mineral dissolution rates as a function of soil depth*
467 A significant observation in this study is the variation of silicate mineral weathering rates as a
468 function of depth in the soil column. As can be seen in Fig. 10, the geometric surface area
469 normalized rates are fastest at the soil surface, and decrease notably just below the surface
470 then increase at the fresh bedrock-soil interface. In some cases, calculated rates, as tabulated
471 in the supplementary material, decrease slightly below zero at intermediate depths between
472 the surface and the bedrock-soil interface. For the case of quartz which does not likely
473 precipitate in low temperature soils, these negative rates, which are low in absolute value, are
474 interpreted to arise due to minor soil composition heterogeneities and analytical uncertainties.
475
476 This variation of rates with depth, and in particular the significantly larger dissolution rates at
477 the base of the soil profiles, is likely the result of a number of factors. First, dissolution rates
478 tend to decrease with the amount of time a mineral surface is exposed to weathering (e.g.

Anderson et al., 2007; Burke et al., 2007; Meunier et al., 2007; White and Brantley, 2003). A decrease in mineral dissolution rates with soil age has been reported for the Merced soil chronosequence by White et al. (1996). This decrease is also qualitatively consistent with the soil production function, which prescribes a decrease in soil production rates with increasing soil depth (Heimsath et al., 1997). A decrease in dissolution rates with weathering duration may be due to both intrinsic and extrinsic factors. Intrinsic factors responsible for this dissolution rate decrease include: 1) a decrease in the relative abundance of reactive minerals and reactive sites on individual mineral grains (Anderson et al., 2007; Hodson et al., 1998; Köhler et al., 2005; Lee et al. 1998; White and Brantley, 2003); and 2) the formation of leached layers and surface coatings that retard the transport of solutes away from the mineral surface (Cubillas et al., 2005; Ganor et al., 2005, Hodson and Langan, 2006; Lee et al., 2008; Meunier et al., 2007; Nugent et al., 1998; Stockmann et al., 2013; White and Brantley, 2003). Extrinsic factors that are potentially responsible for this temporal decrease in dissolution rates include: 1) a reduction in mineral permeability; 2) evolving biologic interactions (Bonneville et al., 2009, 2011; Ehrlich, 1996; Hutchens et al., 2008; Rogers and Bennett, 2004; Stockmann et al., 2012); 3) increases in solute ion concentrations (e.g. Maher, 2010; Schott and Oelkers, 1995; White and Brantley, 2003), and 4) the precipitation of secondary minerals (Ganor et al., 2007; Goddéris et al., 2010; Maher et al., 2009; Moore et al., 2012; Zhu, 2009; Zhu et al., 2004).

The elevated dissolution rates at the top of the soil profile, which contains primary minerals that will have been exposed to the weathering environment for the greatest amount of time are most likely due to the flushing of rain water through the upper soil horizons. This process will maintain the soil pore water at far-from-equilibrium conditions at the surface where

503 dissolution rates are fastest, but closer to equilibrium conditions deeper in the soil profile
504 where rates are slower (c.f. Schott and Oelkers, 1995, Schott et al., 2009, 2012).
505
506 *4.2 Comparison between field and laboratory weathering rates*
507 Plagioclase and potassium feldspar weathering rates determined in the present study are
508 compared with those generated from other field studies in Figs. 12 and 13. Some differences
509 are apparent. It is possible that in many instances these differences stem from the distinct pore
510 fluid compositions and mineral ages of each sample. For example, the values reported in
511 White (2009) are on average somewhat lower that those determined in this study. Pore fluids
512 in that study are somewhat more basic and the minerals are more than > 10000 years old. The
513 lower pH of the Dartmoor and Glen Dye soils, together with the younger age of the Glen Dye
514 soil considered in this study (up to a maximum of 4400 years) may be the origin of these
515 differences. Such differences may also stem from the inherent uncertainties in the
516 determination of field weathering rates; taking account of uncertainties in soil ages, mineral
517 surface areas, and mineral abundance measurements it seems likely that the total uncertainties
518 of dissolution rates of primary minerals in soils determined from field observations are
519 roughly an order of magnitude. Moreover, as rates are strongly dependent on aqueous fluid
520 saturation state, mineral dissolution rates will be influenced strongly by the fluid flow
521 properties in each distinct soil. As such, it is difficult to constrain with confidence the
522 processes leading to differences in mineral dissolution rates obtained from distinct field
523 studies at the present time.
524
525 Also shown in Figs. 12 and 13 are comparisons of rates based on the field observations
526 obtained in this study with corresponding rates obtained in laboratory experiments at 22-25 ºC
527 and 3.5<pH<4.5 taken from the literature. As commonly reported in past studies (Ganor et al.,

2005; Moore et al., 2012; White and Brantley, 2003) the plagioclase, potassium feldspar, and quartz dissolution rates determined in this study from field observations are one or more orders of magnitude lower than those typically reported in laboratory-based studies even accounting for the fact that the majority of these laboratory rates were determined at 25 ºC whereas our field rates were determined for soils that typically experienced lower temperatures. Reasons for the field – laboratory discrepancy have been discussed in detail in the literature (e.g. White and Brantley, 2003) and above in section 4.1.

5. Conclusions

The results summarized above illustrate the complex nature of primary mineral reactivity in soil profiles. The surface area normalized rates were found to vary significantly with depth in the soil profiles. The significantly slower rates of primary mineral dissolution within the soil profile compared to that at either the bedrock interface or the soil surface is particularly significant to soil fertility, as this process is the ultimate source of most nutrients including phosphorus and base cations. As this reduced reactivity can stem from a number of sources, the accurate geochemical modelling of soil fertility remains challenging. In particular, critical to such modelling efforts is whether this slowing in rates stems from 1) changes in pore fluid composition 2) changes in primary mineral surfaces including changes in the number of reactive sites, or 3) the presence of microbes and/or secondary phases on primary minerals surfaces (c.f. Zhu, 2005; Brantley and White, 2009; Maher et al., 2009; Kampman et al., 2009; Steefel and Maher, 2009). Insight into this letter question can be obtained by measuring, in the laboratory element release rates from minerals obtained from natural soils as a function of fluid composition. The results of such measurements will be presented in detail in a future manuscript.

Acknowledgements

This work was supported through a Natural Environment Research Council (NERC) PhD studentship (NE/F016735/1) awarded to the British Geological Survey. Thanks to the Duchy of Cornwall, The Fasque, and Glen Dye Estate for permission to collect samples from their land. Radiocarbon dates were provided via the NERC Radiocarbon facility (Environment), allocation numbers 1518.1010 and 1379,0409 and we thank Dr Charlotte Bryant for advice on sample preparation and analysis. Support from Centre National de la Recherche Scientifique, and the European Community through the MIR Early Stage Training Network (MEST-CT-2005-021120) is gratefully acknowledged. SJK publishes with the permission of the Executive Director, British Geological Survey (NERC). We are also grateful to Andy Tye and Tom Sizmur for their help in the field, Franz Street, Alan Hushcroft, Doris Wagner and Ian Mounteney for their assistance in the laboratory, and Oleg Pokrovsky, Jacques Schott, Gabriella Kakonyi and Therese Flaathen for helpful discussions during the course of this study.

References

Anderson, S.P., Von Blanckenburg, F., White A.F., 2007. Physical and chemical controls on the critical zone. Elements 3, 315–319.

Bain, D. C., Mellor, A., Robertson-Rintoul, M. S. E., Buckland, S. T., 1993. Variations in weathering processes and rates with time in a chronosequence of solids from Glen Feshie, Scotland. Geoderma 67, 275-293,

Banwart A., Bernasconi, S. M., Bloem, J. Blum, W., Brandao, M., Brantley, S.L., Chabaux, F., Duffy, C., Kram, P., Lair, G., Lundin, L., Nikolaos, N., Novak, M., Panagos, P., Ragnarsdottir, K.V., Raynolds, B., Rousseva, S., de Ruiter, P., van Gaans, P., van Riemsdijk, W., White, T., Zhang, B., 2011. Soil processes and functions in critical zone observatories: Hypotheses and experimental design. Vadose Zone J. 10, 974-987.

Bonneville, S., Morgan, D.J., Schmalenberger, A., Bray, A., Brown, A., Banwart, S.A., Benning L.G., 2011. Tree-mycorrhiza symbiosis accelerate mineral weathering: Evidence from nanoscale elemental fluxes at the hypha-mineral interface. Geochim. Cosmochim. Acta 75, 6988-7005.

Bonneville, S., Smits, M.M., Brown, A., Harrington. J., Leake, J.R., Brydson. R., Benning L.G., 2009. Plant-driven fungal weathering: Early stages of mineral alteration at the nanoscale. Geology 37, 615-618.

Boutton T.W., Wong W.W., Hachey D.L., Lee L.S., Cabrera, M.P., Klein, P.D., 1983. Comparison of quartz and pyrex tubes for combustion of organic samples for stable carbon isotope analysis. Anal. Chem. 55, 1832-1833.

Bowen D.Q., Phillips, F.M., Mccabe, A.M., Knuts, P.C., Sykes, G.A., 2002. New data for the last glacial maximum in Great Britain and Ireland, Quat. Sci. Rev. 21, 89-101.

Brady, P.V., 1991. The effect of silicate weathering on global temperature and CO_2. J. Geoph, Res. – Solid Earth. 96, 18101-18106.

Brady, P.V., Carroll, S.A., 1994. Direct effects of CO_2 and temperature on silicate weathering: Possible implications for climate control. Geochim. Cosmochim. Acta 58, 1853-1856.

Brady P. V., Walther J. V., 1990. Kinetics of quartz dissolution at low temperatures. Chem. Geol. 82, 253-264.

Brantley, S.L., Buss, H., Lebedeva, M., Fletcher, R.C., Ma, L., 2011. Investigating the complex interface where bedrock transforms to regolith. App. Geochem. 26, S12-S15.

Brantley, S.L., White, A.F., 2009. Approaches to modeling weathered regolith. Rev. Min. Geochem. 70, 435-484.

Braun, J.-J., Marchal, J. C., Riotte, J., Bogglin, J. L., Bedimo, J. P. B., Ngoupayou, J. R. N., Nyeck, B., Robain, H., Sekhar, M., Audry, S., Viers, J., 2012. Elemental weathering fluxes and saprolite production rate in a Central African lateric terrain (Nsimi, South Cameroon). Geochim. Cosmochim. Acta 99, 243-270.

Brunauer, S., Emmett, P. H., Teller, E., 1938. Adsorption of gases in multimolecular layers. J. Am. Chem. Soc. 60, 309-319.

Burke, B. C., Heimsath, A.M., White, A.F., 2007. Coupling chemical weathering with soil production across soil-mantled landscapes. Earth Surf. Process. Land. 32, 853-873.

Buss, H. L., Sak, P.B., Webb, S. M., Brantley, S.L., 2008. Weathering of the Rio Blanco quartz diorite, Luquillo Mountains, Puerto Rico: Coupling oxidation, dissolution, and fracturing. Geochim. Cosmochim. Acta, 72, 4488-4507.

Casey, W.H., Westrich, H.R., Holdren, G.R., 1991. Dissolution of plagioclase at pH = 2 and 3. Amer. Min. 76, 211-217.

Cheng, P., Zhou, W.J., Wang, H., Lu, X.F., Du, H., 2013. ^{14}C dating of soil organic carbon (SOC) in Loess-Paleosol using sequential pyrolysis and accelerator mass spectrometry (AMS). Radiocarbon, 55, 563-570.

Chesley, J.T., Halliday, A.N., Snee, L.W., Mezger, H., Shepherd, T.J., Scrivener, R.C., 1993. Thermochronology of the Cornubian batholiths in southwest England: Implications for pluton emplacement and protracted hydrothermal mineralization. . Geochim. Cosmochim. Acta 57, 1817-1835.

Clow, D.W., Drever, J.I., 1996. Weathering rates as a function of flow through an alpine soil. Chem. Geo. 132, 121-141.

Cubillas P., Köhler S., Prieto M., Causserand C., Oelkers E. H., 2005. How do mineral coatings affect dissolution rates? An experimental study of coupled $CaCO_3$ dissolution – $CdCO_3$ precipitation. Geochim. Cosmochim. Acta 69, 5459–5476.

De Boer, G.B.J, de Weerd, C., Thoenes, D., Gossens,H. W. J., 1987. Laser diffraction spectrometry: Fraunhofer diffraction versus Mie scattering: Particle Characterization 4, 14–19.

Deer, W., Howie, R.A., Zussman, J., 2013. An introduction to the rock forming minerals. Mineralogical Society. Pp 505.

636 Dere, A.L., White, T.S., April, R.H., Reynolds, B., Miller, T.E., Knapp. E.P., McKay, K.D.,
637 Brantley, S.L., 2013. Climate dependence of feldspar weathering in shale soils along a
638 latitudinal gradient. Geochim. Cosmochim. Acta 122, 101-126.

639 Dequincey, O., Chabaux, F., Clauer, N., Liewig, N., Muller, J.-P., 1999. Dating of weathering
640 profiles by radioactive disequilibria: Contribution of the study of authigenic mineral
641 fractions. Comptes Rendus de l'Académie des Sciences – Series IIA – Earth and
642 Planetary Science 328, 679-685.

643 Dixon, J.L, Heimsath, A.M., Amundson, R., 2009. The critical role of climate and saprolite
644 weathering in landscape evolution. Earth Surface Processes and Landforms 34, 1507-
645 1521.

646 Dixon J.L., von Blanckenburg, F., 2012. Soil as pacemakers and limiters of global silicate
647 weathering. Comp. Rend. Geosci. 344, 597-609.

648 Dove, P.M., 1994. The dissolution kinetics of quartz in sodium chloride solutions at 25° to
649 300° C Am. J. Sci. 294, 665-712.

650 Dreibrodt, S., Jarecki, H., Lubos, C., Khamnueva, S.V., Klamm, M., Bork, H.-R., 2013.
651 Holocene soil formation and soil erosion at a slope beneath the Neolithic earthworm
652 Salzmünde (Saxony-Anhalt, Germany). Catena 107, 1-14.

653 Drever J.I., Clow, D.W., 1995. Weathering rates in catchments. Rev. Min. 31, 463-483.

654 Egli, M., Mirabella, A., Sartori, G., Fitze, P., 2003. Weathering rates as a function of climate:
655 Results from a climosequence of the Val Genova (Trentino Italian Alps). Geoderma
656 111, 99-121.

657 Ehrlich, H.L., 1996. How microprobes influence mineral growth and dissolution. Chem. Geo.
658 132, 5-9.

659 Exley C.S., Stone, M., 1964. The granitic rocks of south-west England. In: Hosking F. K. G.
660 and Shrimpton, G. I. (eds.) Present Views of some aspects of the Geology of Cornwall
661 and Devon. Truro.

662 Favilli, F., Egli, M., Brandova, D., Ivy-Ochs, S., Kubik, P., Cherubini, P., Mirabella, A.,
663 Sartori, G., Giaccai, D., Haeberli, W., 2009. Combined use of relative and absolute
664 dating techniques for detecting signals of Alpine landscape evolution during the late
665 Pleistocene and early Holocene. Geomorphology 112, 48-66.

666 Freeman, S.P.T., Cook, G.T., Dougans, A.B., Naysmith, P., Wilcken, K.M.,
667 Xu, S., 2010. Improved SSAMS performance. Nuclear Instruments and Methods in
668 Physics Research Section B268, 715-717.

669 Gaillardet, J., Dupre, B., Louvat, P., Allegre, C.J., 1999. Global silicate weathering and CO_2
670 consumption rates deduced from the chemistry of large rivers. Chem. Geo. 159, 3-30.

671 Ganor J., Lu P., Zheng Z. P., Zhu C., 2007. Bridging the gap between laboratory
672 measurements and field estimations of silicate weathering using simple calculations.
673 Environ. Geol. 53, 599- 610.

674 Ganor, J., Roueff, E., Erel, Y., Blum, J. D., 2005. The dissolution kinetics of a granite and its
675 minerals: Implications for comparison between laboratory and field dissolution rates.
676 Geochim. Cosmochim. Acta 69, 607-621.

677 Gautier, J.-M., Oelkers, E.H., Schott, J., 2001. Are quartz dissolution rates proportional to
678 B.E.T. surface area? Geochim. Cosmochim. Acta 65, 1059-1070.

679 Gislason S. R., Arnórsson S., Armannsson H., 1996. Chemical weathering of basalt as
680 deduced from the composition of precipitation, rivers, and rocks in SW Iceland. Am. J.
681 Sci. 296, 837-907.

682 Gislason, S.R., Oelkers E.H., Snorrason Á., 2006. The role of river suspended material in the
683 global carbon cycle. Geology 34, 49-52.

684 Gislason, S. R., Oelkers, E. H., Eiriksdottir, E. S., Kardjilov, M. I., Gisladottir, G., Sigfusson,
685 G., Snorrason, A., Elefsen, S., Hardardottir, J., Torssander, P., Oskarsson N., 2009.
686 Direct evidence of the feedback between climate and weathering. Earth Planet. Sci. Let.
687 277, 213-222.

688 Godderis, Y., Williams, J.Z., Schott, J., Pollard, D., Brantley.S.L., 2010. Time evolution of
689 the mineralogical composition of Mississippi Valley loess over the last 10 kyr: Climate
690 and geochemical modeling. Geochim. Cosmochim. Acta 74, 6357-6374.

691 Gudbrandsson, S., Wolff-Boenisch, D., Gislason, S.R., Oelkers, E.H., 2011. An experimental
692 study of crystalline basalt dissolution from $2 \leq pH \leq 11$ and temperatures from 5 to 75
693 °C. Geochim. Cosmochim. Acta 75, 5496-5509.

694 Harkness, D. D., Wilson, H.W., 1972. Some applications in radiocarbon measurement at the
695 SURRC. In: Proceedings of Eighth International Conference on Radiocarbon Dating.
696 Royal Society of New Zealand B101-B115.

697 Hartman, J., Moosdorf, N., Lauerwald, R., Hinderer, M., West, A. J., 2014. Global chemical
698 weathering and associated P-release – The role of lithology, temperature and soil
699 properties. Chem. Geol. 363, 145-163.

700 Hausrath E. M., Navarre-Sitchler A. K., Sak P. B., Williams J. Z., and Brantley S. L., 2011.
701 Soil profiles as indicators of mineral weathering rates and organic interactions for a
702 Pennsylvania diabase. Chem Geo. 290, 89-100.
703 Heimsath, A.M., DiBiase, R.A., Whipple, K.X., 2012. Soil production limits and the
704 transition to bedrock-dominated landscapes. Nature Geosci. 5, 210-214.

705 Heimsath, A.M., Dietrich, W. E., Nishiizumi, K., Finkel, R. C., 1997. The soil production
706 function and landscape equilibrium. Nature 388, 358–361

707 Hiruma, S. T., Modenesi-Gauttieri, M. C., Riccomini, C., 2013. Late Quaternary colluvial
708 deposits in the Bocaina Plateau, southeastern Brazil highlands: age and
709 palaeoenvironmental consequences. Boreas 42, 306-316.

710 Hodson, M.E., 2006. Does reactive surface area depend on grain size ? Results from pH 3, 25
711 °C far-from-equilibrium flow-through dissolution experiments on anorthite and
712 biotite. Geochim. Cosmochim. Acta 70, 1655-1667

713 Hodson, M.E., 2002. Experimental evidence for mobility of Zr and other trace elements in
714 soils. Geochim. Cosmochim. Acta 66, 819 – 828

715 Hodson, M.E., Langan, S. J., 1999. The influence of soil age on calculated mineral weathering
716 rates. App. Geochem. 14, 387-3904.

717 Hodson, M.E., Langan, S. J., Kennedy, F. M., Bain, D.C., 1998. Variation in soil surface area
718 in a chronosequence of soils from Glen Feshie, Scotland and its implications for mineral
719 weathering rate calculations. Geoderma 85, 1-18.

720 Hutchens, E., Valsami-Jones, E., Harouiya, N., Chairat, C., Oelkers, E.H., McEldoney, S.,
721 2008. An experimental investigation of Bacillus megaterium on apatite dissolution.
722 Geomicrobio. J. 23, 177-182.

723 Kaiser, K., Eusterhues, K., Rumpel, C., Guggenberger G., Kogel-Knabner, I., 2002.
724 Stabilizaion of organic matter by soil minerals: Investigation of density and particle-size
725 fractions from two acid forest soils. J. Plant Nut. Soil Sci. 165, 451-459.

726 Kampman, N., Bickle, M., Becker, J., Assayag, N., Chapman, H., 2009. Feldspar dissolution
727 kinetics and Gibbs free energy dependence in a CO_2-enriched groundwater system,
728 Green River, Utah. Earth Planet. Sci. Let. 284, 473-488.

729 Klaminder, J., Lucas, R.W., Futter, M.N., Bishop, K.H., Köhler S. J., Egnell, G., Laudon, H.,
730 2011. Silicate mineral weathering rate estimates: Are they precise enough to be useful
731 when predicting the recovery of nutrient pools after harvesting? Forest Ecol. Manag.
732 261, 1-9.

733 Kemp, S.J., Merriman, R.J., 2009. Polyphase low-grade metamorphism of the Ingleton Group,
734 northern England, U.K.: A case study of metamorphic inversion in a mudrock
735 succession. Geol. Mag. 146, 237-251.

736 Köhler S. J., Bosbach D., Oelkers E. H., 2005. Do clay mineral dissolution rates reach steady-
737 state? Geochim. Cosmochim. Acta 69, 1997-2006.

738 Kump L. R., Brantley S. L., Arthur M. A., 2000. Chemical weathering, atmospheric CO_2, and
739 climate. Ann. Rev. Earth Planet. Sci. 28, 611-667.

740 Kurtz A. C., Derry L. A., Chadwick O. A., Alfano M. J., 2000. Refractory element mobility in
741 volcanic soils. Geology 28, 683–686.

742 Lee, M. R., Hodson, M.E., Parsons, I., 1998. The role of intragranular microtextures and
743 microstructures in chemical and mechanical weathering: direct comparisons of
744 experimentally and naturally weathered alkali feldspars. Geochim. Cosmochim. Acta
745 62, 2771 - 2788.

746 Lee, M. R, Hodson, M.E., Brown, D.J., MacKenzie, M., Smith, C.L., 2008. The composition
747 and crystallinity of the near-surface regions of weathered alkali feldspars. Geochim.
748 Cosmochim. Acta 72, 4962 - 4975.

749 Ma, L., Jin, J., Brantley, S.L., 2011. How mineralogy and slope aspect affect REE release and
750 fractionation during shale weathering in the Susquehanna/Shale Hills Critical Zone
751 Observatory. Chem. Geo. 290, 31-49.

752 Madsen, I.C., Scarlett, N.V.Y., 2008. Quantitative Phase Analysis. In Powder Diffraction:
753 Theory and Practice, edited by Dinnebier, R.E. and Billinge, S.J.L., Royal Society of
754 Chemistry, pp298-331.

755 Maher, K., 2010. The dependence of chemical weathering rate on fluid residence time. Earth.
756 Planet. Sci. Let. 294, 101-110.

757 Maher, K., Steefel. C.I., White, A.F., Stonestrom, D.A., 2009. The role of reaction affinity
758 and secondary minerals in regulating chemical weathering rates at the Santa Cruz
759 chronosequence, California. Geochim. Cosmochim. Acta 73, 2804-2831.

760 Maher, K., Steefel, C.I., DePaolo, D.J., 2004. U-234/U-238 disequilibrium as a measure of
761 weathering rates in soils and sediments. Geochim. Cosmochim. Acta 68, A416.

762 Manley, P., Evans, L.J., 1986. Dissolution of feldspars by low molecular weight aliphatic and
763 aromatic acids. Soil Sci. 141, 106-112.

764 Martin, C.W., Johnson, W.C., 1995. Variation in radiocarbon ages of soil organic-matter from
765 late quaternary buried soils. Quaternary Res., 43, 232-237.

766 Matthews, J.A., Dresser, P.Q., 1983. Intensive ^{14}C dating of a buried paleosol horizon.
767 Geolog. Foren. Stochholm Forhand. 105, 59-63.

768 McClelland, J.E., 1950. The effect of time, temperature and particle size on the release rates
769 of bases from some common soil-forming minerals of different crystal structure. Soil.
770 Sci. Soc. Proc. 15, 301-301.

771 Meunier, A., Sardini, P., Robinet, J. C., Pret, D., 2007. The petrography of weathering
772 processes: Facts and outlooks. Clay Minerals 42, 415-435.

773 Montgomery, D.R., 2007. Soil erosion and agricultural sustainability. Proc. Nat. Acad. Sci.
774 104, 13268-13272.

775 Moore J., Lichtner P. C., White A. F., Brantley S. L., 2012. Using a reactive transport model
776 to elucidate differences between laboratory and field dissolution rates in regolith.
777 Geochim. Cosmochim. Acta 93, 235-261.

778 Moquet, J.-S., Crave, A., Viers, J., Seyler, P., Armijos, E., Bourrel, L., Chavarri, E., Lange,
779 C., Laraquem A., Casimiro, W.S.L., Pombosa, R., Noriges, L., Vera, A., Guyot, J.L.,
780 2011. Chemical weathering and atmospheric/soil CO_2 uptake in the Andean and
781 Foreland Amazon basins. Chem. Geo. 287, 1-26.

782 Navarre-Sitchler, A. K., Cole, D. R., Rother, G., Jin, L., Buss, H. L., Brantley, S.L., 2013.
783 Porosity and surface area evolution during weathering of two igneous rocks. Geochim.
784 Cosmochim. Acta 109, 400-413.

785 Norton, N.P., von Blanckenburg, F., 2010. Silicate weathering of soil-mantled slopes in an
786 active Alpine landscape. Geochim. Cosmochim. Acta 74, 5243-5258.

787 Nugent, M. A., Brantley, S. L., Pantano, C. G., Maurice, P.A., 1998. The influence of natural
788 mineral coatings on feldspar weathering. Nature 395, 588-591.

789 Oliva. P., Viers, J., Dupre, B., 2003. Chemical weathering in granitic environments. Chem.
790 Geo. 202, 225-256.

791 Oxburgh, R. Drever, J.L., Sun, Y.T., 1994. Mechanism of plagioclase dissolution in acid
792 solution at 25 ºC. Geochim. Cosmochim. Acta 58, 661-669.
793 Parry, S.A., 2012. Turning rock into soil –variations in soil mineral reactivity, surface area
794 and porosity through the critical zone. Unpublished PhD thesis, University of Reading.

795 Pressenda, L.C.R., Gouveia, S.E.M., Aravena, R., 2001. Radiocarbon dating of total soil
796 organic matter and humic fraction and its comparison with ^{14}C ages of fossil charcoal.
797 Radiocarbon, 43, 595-601.

798 Price, J.R., Vebel, M.A., 2003. Chemical weathering indices applied to weathering profiled
799 developed on heterogeneous felsic metamorphic rocks. Chem. Geol. 202, 397-416.

800 Rasmussen, C., Brantley, S. L., Richter, D.D., Blum, A., Dixon, J., White, A.F., 2011. Strong
801 climate and tectonic control on plagioclase weathering in granitic terrain. Earth. Planet.
802 Sci,. Let. 301, 521-530.

803 Reheis, M. C., 1990. Influence of climate and eolian dust on the major element chemistry and
804 clay mineralogy of soils in the northern Bighorn basin U.S.A. Catena 17, 219-248.

805 Ricker, M.C., Donohue, S.W., Stolt, M.H., Zavada, M.S., 2012. Development and application
806 of multi-proxy indices of land use change for riparian soils in southern New England,
807 USA. Ecological Applications 22, 487-501.

Riggins, S.G., Anderson, R. S., Anderson, S. P., Tye, A.M., 2011. Solving a conundrum of a steady-state hilltop with variable soil depths and production rates, Bodmin Moor, UK. Geomorphology 128, 73-84.

Rogers, J.R., Bennett, P.C., 2004. Mineral stimulation of subsurface microorganisms: Release of limiting nutrients from silicates. Chem. Geo. 203, 91-108.

Rowell, D. L., 1994. Soil Science: Methods and Applications. Longman Scientific & Technical, Essex, England.

Salehikhoo, F., Li, L., and Brantley, S.L., 2013. Magnesite dissolution rates at different spatial scales: The role of mineral spatial distribution and flow velocity. Geochim. Cosmochim. Acta 108, 91-106.

Schaller, M., Blum, J. D., Hamburg, S.P., Vadeboncoeur, M.A., 2010. Spatial variability of long-term chemical weathering rates in the White Mountains, New Hampshire, USA. Geoderma 154, 294-301.

Scharpenseel, H.W., Becker Heidmann, P., 1992. Twenty-five years of radiocarbon dating soils: paradigm of erring and learning. Radiocarbon 34, 541-549.

Schott J., Oelkers E.H., 1995. Dissolution and crystallization rates of silicate minerals as a function of chemical affinity. Pure App. Chem. 67, 903-910.

Schott, J. Oelkers, E.H., Benezeth, P. Godderis, Y., Francois, L., 2012. Can accurate kinetic laws be created to describe chemical weathering ? Comptes. Rendus Geosci. 344, 568-585.

Schott, J., Pokrovsky, O.S., Oelkers, E.H., 2009. The link between mineral dissolution/precipitation kinetics and solution chemistry. Rev. Min. Geochem. 70, 207-258.

Schweda, P., 1990. Kinetics and mechanisms of alkali feldspar dissolution at low temperatures, PhD dissertation, Stockholm University.

Sharp, W.D., Ludwig, K.R., Chadwick, O.A., Amundson, R., Glaser, L.L., 2003. Dating fluvial terraces by ^{230}Th/U on pedogenic carbonate, Wind River Basin, Wyoming. Quaternary Res. 59, 139-150.

Slota, P.J., Jull, A.J.T., Linick, T.W., Toolin, L.J., 1987. Preparation of small samples for ^{14}C accelerator targets by catalytic reduction of CO. Radiocarbon 29, 303-306.

Snyder, R.L., Bish, D.L., 1989. Quantitative analysis. Rev. Min. 20, 101-144.

Soulsby, C., Rodgers, P.J., Petry. J., Hanna, D.M., Malcolm, I.A., Dunn, S.M., 2004. Using tracers to upscale flow path understanding in mesoscale mountainous catchments: Two examples from Scotland. J. Hydro. 281, 174-196.

Steefel, C.I., Maher, K., 2009. Fluid-rock interaction: A reactive transport approach. Rev. Min. Geochem. 70, 485-532.

Stillings, L.L., Brantley, S.L., 1995. Feldspar dissolution at 25 °C and pH 3: reaction stoichiometry and the effect of cations. Geochim. Cosmochim. Acta 59, 1483-1496.

Stillings, L.L., Drever, J.I., Brantley, S.L., Sun, Y., Oxburgh, R., 1996. Rates of feldspar dissolution at pH 3-7 with 0-8 mM oxalic acid. Chem. Geo. 132, 79-90.

Stockmann, G.J., Shirokova, L.S., Pokrovsky, O.S., Benezeth, P., Bovet, N., Gislason. S.R., Oelkers, E.H., 2012. Does the presence of heterotrophic bacterium Pseudomonas reatans affect basaltic glass dissolution rates? Chem. Geo. 296, 1-18.

Stockmann, G. J., Wolff-Boenisch D., Gislason, S. R., Oelkers, E. H., 2013. Do carbonate precipitated affect dissolution kinetics?: 2. Diopside. Chem. Geo. 337-338, 56-66.

Stuiver, M., Polach, H.A., 1977. Discussion: Reporting of ^{14}C data. Radiocarbon 19, 355 – 363.

Stutter, M.I., Deeks, L. K., Billett, M.F., 2004. Spatial variability in soil exchange chemistry in a granitic upland catchment. Soil Sci. Soc. Am. J. 68, 1304-1314.

Sverdrup, H., 1990. The kinetics of Base Cation Release due to Chemical Weathering. Lund University Press.

Sverdrup H., Rosen. K., 1998. Long term base cation balances for Swedish forests and the concept of sustainability. Forest Ecol. Manag. 110, 221-236.

Sverdrup, H., Thelin, G., Robles, M., Stjernquist, I., Sorenjen, J., 2006. Assessing nutrient sustainability of forest production for different tree species considering Ca, Mg, K, N and P at Bjornstorp Estate,Sweden. Biogeochem. 81, 219-238.

Swindale L. D., Jackson M. L., 1956. Genetic processes in some residual podzolised soils of New Zealand. 6th Soil Science Congress, Paris, Vol. 37, 233–239. International Union of Soil Sciences.

Tester, J.W., Worley, W.G., Robinson, B.A., Grigsby, C.O., Freerer, J.L., 1994. Correlating quartz dissolution kinetics in pure water from 25 to 625 ºC. Geochim. Cosmochim. Acta 58, 2407-2420.

Tonneijck, F.H., van de Plicht, J., Jansen, B., Vertraten, J.M., Hooghiemstra, H., 2006. Radiocarbon dating of soil organic matter fractions in Andasols in northern Ecuador. Radiocarbon, 48, 337-353.

Turpault, M.-P., Trotignon, L., 1994. The dissolution of biotite single crystals in dilute HNO_3 at 24 °C: evidence of an anisotropic corrosion process of micas in acidic solutions. Geochim. Cosmochim. Acta 58, 2761-2775.

Viers J., Dupre B., Braun J. -J., Deberdt S., Angeletti B., Ngoupayou, J. N., Michard A., 2000. Major and trace element abundances, and strontium isotopes in the Nyong basin rivers (Cameroon): Constraints on chemical weathering processes and elements transport mechanisms in humid tropical environments. Chem. Geol. 169, 211–241.

Volk, T., 1987. Feedbacks between weathering and atmospheric CO_2 over the last 100 million years. Am. J. Sci. 287, 763-779

Wakabayshi, S., Matsuzaki, H., Miyairi, Y., Asano, M., Tamura, K., 2012. Chrinology of anthropedogenesis in the Omiya tableland, Japan, based in a ^{14}C age profile of humic acid. Soil Sci. Plant Nutrit. 58, 737-749.

Walker, J.C.G., Hays, P.B., Kasting, J.F., 1981. A negative feedback mechanism for the long-term stabilization of Earth's surface temperature. J. Geoph. Res. – Oceans and Atmosphere 86, 9776-9782.

Wang, Y., Amundson, R., Trumbore, S., 1996. Radiocarbon dating of soil organic matter. Quaternary Res. 45, 282-288.

Welch, S.A., Ullman, W.J., 1996. Feldspar dissolution in acidic and organic solutions. Compositional and pH dependence of dissolution rate. Geochim. Cosmochim. Acta 60, 2939-2948

White, A.F., 2002. Determining the weathering rates based on solid and solute weathering gradients and velocities: Application to biotite weathering in saprolites. Chem. Geo. 190, 69-89.

White, A.F., 2009. Natural weathering rates of silicate minerals. Pp 133-168. In: Surface and ground water, weathering and soils (ed. J.I. Drever). Vol 5 Treatise on Geochemsitry (eds. H.D. Holland and K.K. Turekian), Elsevier-Pergamon, Oxford.

White, A.F., Blum, A.E., 1995. Effects of climate on chemical weathering rates in watersheds. Geochim. Cosmochim. Acta 59, 1727-1736.

White, A.F., Blum, A.E., Schulz, M.S., Bullen, T.D., Harden, J.W., Peterson, M.L., 1996. Chemical weathering of a soil chronosequence on granitic alluvium. I. Quantification of mineralogical and surface area changes and calculation of primary silicate reaction rates. Geochim. Cosmochim. Acta 60, 2533-2550.

White, A. F., Brantley, S. L., 2003. The Effect of time on the weathering of silicate minerals: Why do weathering rates differ in the laboratory and field? Chem. Geo. 202, 479-506.

White A.F., Bullen, T.D., Schulz, M. S., Blum, A.E., Huntington, T.G., Peters, N. E., 2001. Differential rates of feldspar weathering in granitic regoliths. Geochim. Cosmochim. Acta 65, 847-869.

White, A.F., Schulz, M.S., Stonestrom, D.A., Vivit, D.V., Fitzpratic, J., Bullen, T.D., Haher, K. Blum, A.E. 2008. Chemical weathering of a marine terrace chronosequence, Santa Cruz, California. Part I: Interperting rates and controls based on soil concentration-depth profiles. Geochim. Cosmochim. Acta, 72, 36-68.

White, A.F., Schulz, M.S., Stonestrom, D.A., Vivit, D.V., Fitzpratic, J., Bullen, T.D., Haher, K. Blum, A.E. 2009. Chemical weathering of a marine terrace chronosequence, Santa Cruz, California. Part II: Solute profiles, gradiants and the comparisons of long-term weathering rates. Geochim. Cosmochim. Acta, 73, 2769-2803.

Wollast, R., 1967. Kinetics of alteration of K-feldspar in buffered solutions at low temperature. Geochim. Cosmochim. Acta 31, 635-648.

Young, R.A., 1993. The Rietveld Method, Oxford University Press, Oxford U.K.

Zhu, C. 2005. In situ feldspar dissolution rates in an aquifer. Geochim. Cosmochim. Acta 69, 1435-1453.

Zhu, C., 2009. Geochemical modeling of reaction paths and geochemical reactions networks. Rev. Min. Geochem. 70, 533-569.

Zhu C., Blum A. E., Veblen D. R., 2004. Feldspar dissolution rates and clay precipitation in the Navajo aquifer at Black Mesa, Arizona, USA. In *Proceedings of the Eleventh International Symposium on Water-Rock Interaction* (eds. R. Wanty and R. Seal, II). A. A. Balkema Publishers, Philadelphia. pp. 895-899

Zollinger, B., Alewell, C., Kneisel, C., Meusburger, K., Gärtner, H., Brandová, D., Ivy-Ochs, S., Schmidt, M.W.I. and Egli, M., 2013. Effect of permafrost on the formation of soil organic carbon pools and their physical-chemical properties in the Eastern Swiss Alps. Catena 110, 70-85.

Figure Captions

Fig. 1. Location of the Dartmoor (DM02) and Glen Dye (GD02) sampling sites considered in this study. The dashed line shows the southernmost extent of ice during the most recent glacial maximum.

Fig. 2. a) Geometric and b) BET surface area of the DM02 and GD02 soil profiles following removal of organic material.

Fig. 3. Variation in a) organic matter content and b) pH with depth in the DM02 and GD02 soil profiles. (n = 3, error bars = standard deviation).

Fig. 4. The elemental chemistry of the bulk soil and bedrock normalised to 100 % at the a) DM02 and b) GD02 sites as determined by XRFS as a function of depth. Data plotted at 95 cm are for the altered bedrock and at 100 cm for the unaltered bedrock.

Fig. 5. Ti concentrations of the bulk soil and bedrock normalised to 100 % at the a) DM02 and b) GD02 sites as determined by XRFS as a function of depth. Data plotted at 95 cm are for the altered bedrock and at 100 cm for the unaltered bedrock

Fig. 6. Variation of mineralogy with depth for the a) DM02 and b) GD02 soil profiles and bedrock. Organic matter was removed from the samples by oxidation prior to analysis. Data plotted at 95 cm are for the altered bedrock and at 100 cm for the unaltered bedrock.

Fig. 7. The a) element and b) mineral phase τ plots for the DM02 soil profile. Data plotted at 95 cm are for the altered bedrock.

Fig. 8. The a) element and b) mineral phase τ plots for the GD02 soil profile. Data plotted at 95 cm are for the altered bedrock.

Fig. 9. Radiocarbon age of bulk soil humin fraction against sample depth in the a) DM02 and b) GD02 soil profiles. Weighted linear regression trend lines used 3 and 6 data points in the DM02 and GD02 soil profiles, respectively.

Fig. 10. The variation of the calculated mineral dissolution rates normalised to geometric surface area with sample depth in the a) DM02 and b) GD02 soil profiles.

Fig. 11. The variation of the calculated mineral dissolution rates normalised to BET surface area with sample depth in the a) DM02 and b) GD02 soil profiles.

Fig. 12. A comparison of the plagioclase dissolution rates determined in this study and those reported in the literature. Rates are normalised to a) geometric and b) BET surface area. Literature field rates are taken from Table 2 in White (2009), whereas literature laboratory rates for intermediate plagioclases at 22-25 ºC and 3.5<pH<4.5 were taken from Casey et al., (1991), Welch and Ullmann (1993), Oxburgh et al. (1994), and Stillings et al. (1996).

967 Note that much of the literature data were available as either BET or geometric surface
968 area normalized rates, so do not appear in both plots.
969 **Fig. 13.** A comparison of the rates determined in this study and those reported in the
970 literature. Rates are normalised to a) geometric surface area normalized K-feldspar rates,
971 b) BET surface area normalized K-feldspar rates, and c) BET surface area normalized
972 quartz rates. Literature 'field' rates are taken from Table 2 in White (2009), whereas
973 literature laboratory rates for temperatures from 22 to 25 °C and 3.5<pH<4.5 were taken
974 from McCelland (1950), Wollast (1967), Manley and Evans (1986), and Schweda (1989)
975 for K-feldspar, and Brady and Walther (1990), Sverdrup (1990), and Dove (1994) for
976 quartz. Note that much of the literature data were available as either BET or geometric
977 surface area normalized rates, so do not appear in both plots.
978
979

980 Table 1 : Stratigraphic descriptions of the sampled solids considered in this study
981

Depth / cm	Horizon	Description	Matrix Colour
DM02			
0 - 17	O	Amorphous peat horizon	10Yr 2/1 (Black)
17 - 27	Ae	Bleached horizon, light grey matrix with bleached white patches.	10Yr 4/2 (Dark Greyish Brown)
27 - 42	Bs	Iron rich horizon, with potential iron pan	10Yr 6/8 (Brownish Yellow)
42 - 50	B	Mineral horizon, light brown / orange matrix with black mottles.	10Yr 5/3 (Brown)
50 - 91	C	Darker brown, mineral rich horizon, with more limited mottling.	10Yr 4/3 (Brown)
>91	R	Regolith / Altered Bedrock	
GD02			
0 - 40	O	Amorphous peat horizon	10Yr 2/1 (Black)
40 - 50	Ae	Very fine silty matrix at O horizon boundary, becoming coarser within a 2cm underlying the interface. Potentially an Ae horizon as white mineral grains, probably quartz, dominate the soil colour, relative to the underlying Bt horizon.	10Yr 8/2 (Very Pale Brown)
50 - 60	Bt	Finer texture than overlying Ae horizon, with increasing silt and clay fractions.	7.5Yr 4/2 (Brown)
60 – 81	C	Unconsolidated C horizon.	10Yr 6/6 (Brownish Yellow)
>81	R	Regolith / Altered Bedrock	10Yr 5/4 (Yellowish Brown)

O = a horizon dominated by organic material consisting of undecomposed or partially decomposed litter.
Ae = a mineral horizon in which much of the original rock structure has been obliterated showing moderately decomposed organic matter.

Bt = a mineral horizon that has lost all or much of the original rock structure and is showing illuvial accumulation of silicate clay.

Bs = a mineral horizon that has lost all or much of the original rock structure and is showing an illuvial accumulation of sesquioxides.

B = a mineral horizon that has lost all or much of the original rock structure.

C = a horizon that is little affected by the pedogenic process
R = a hard bedrock

982
983

984

985

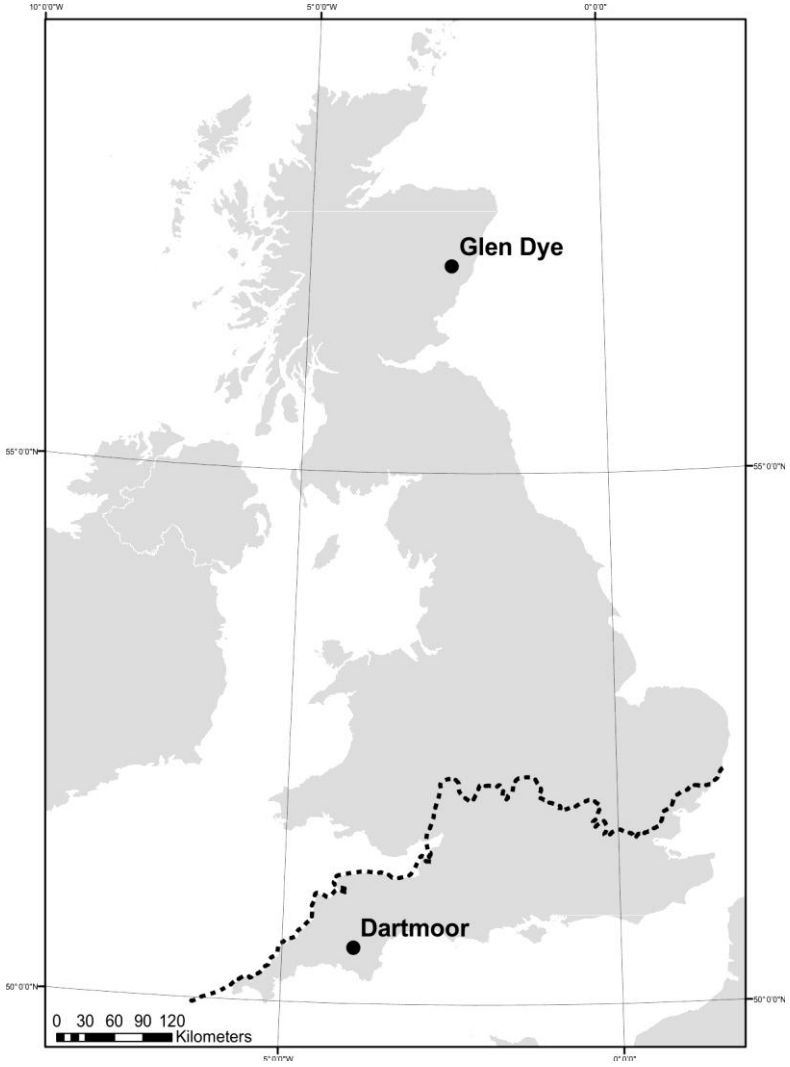

Fig. 1. Location of the Dartmoor (DM02) and Glen Dye (GD02) sampling sites considered in this study. The dashed line shows the southernmost extent of ice during the most recent glacial maximum.

994 a.

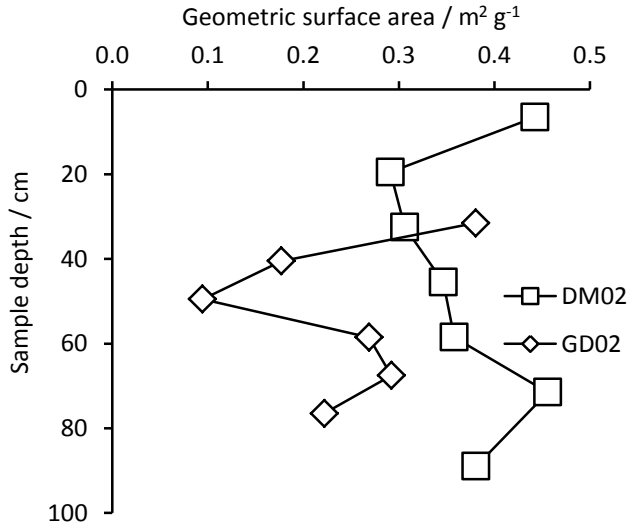

995

996 b.

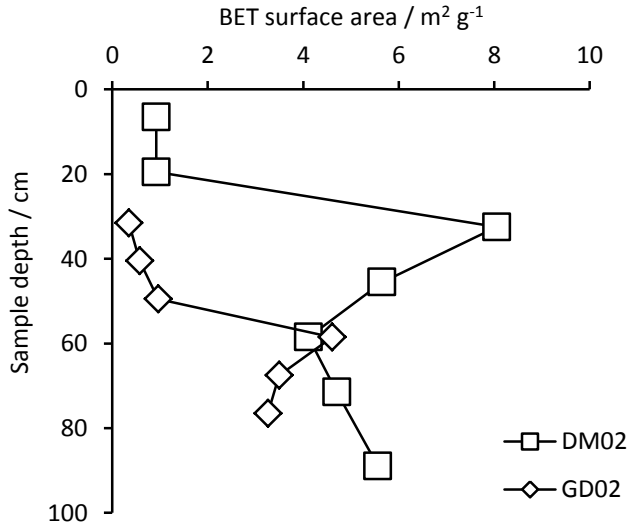

997

998

999 **Fig. 2.** a) Geometric and b) BET surface area of the DM02 and GD02 soil profiles following
1000 removal of organic material.

1001

a.

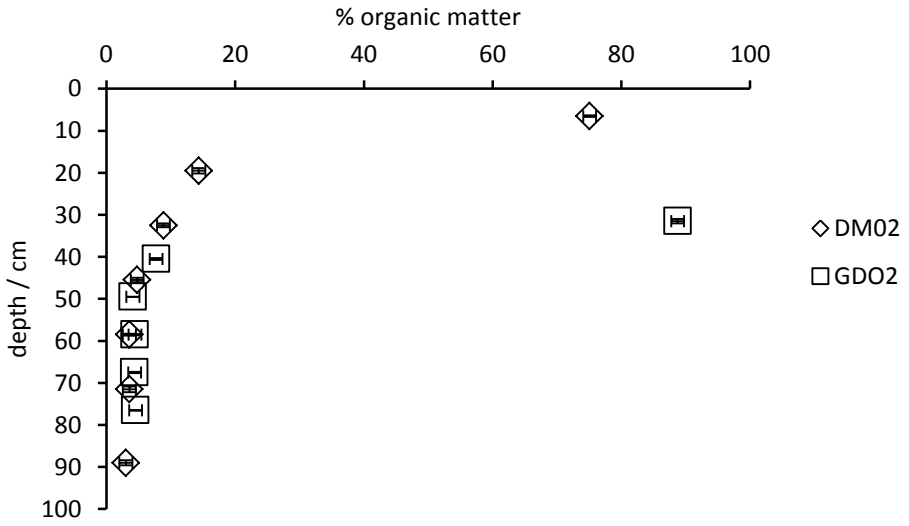

b.

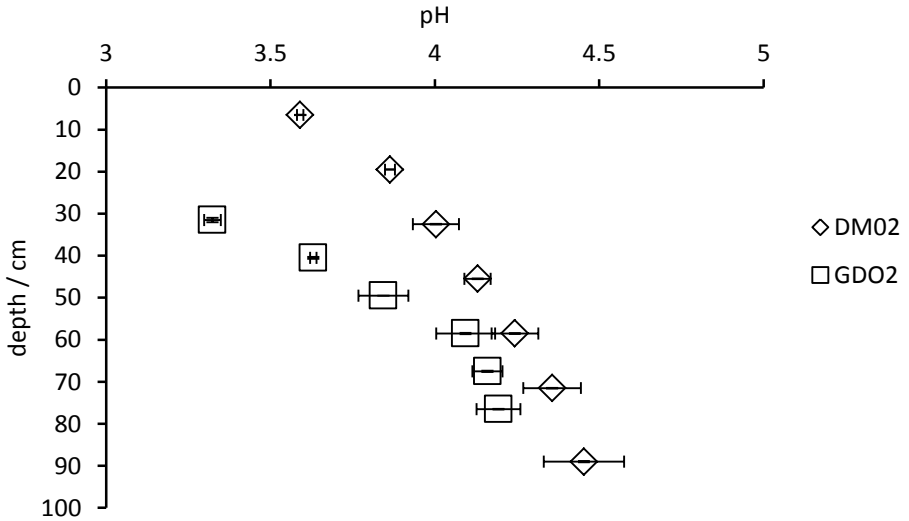

Fig. 3. Variation in a) organic matter content and b) pH with depth in the DM02 and GD02 soil profiles. (n = 3, error bars = standard deviation).

a.

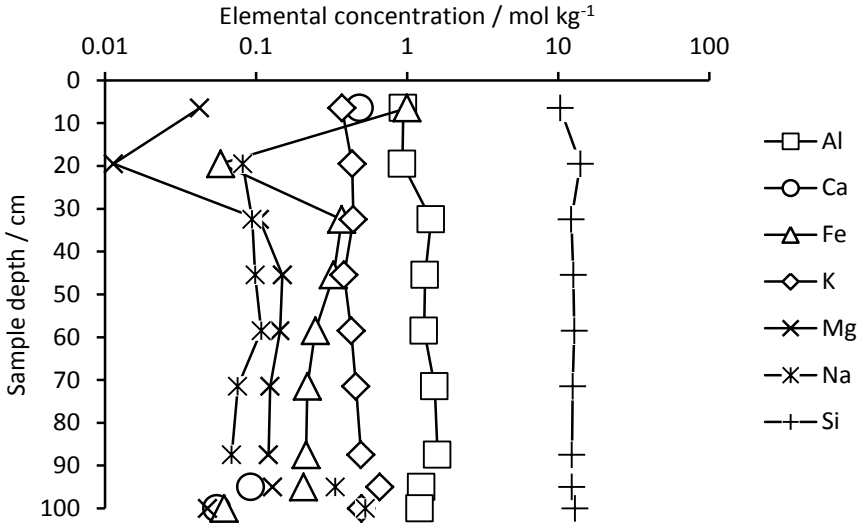

b.

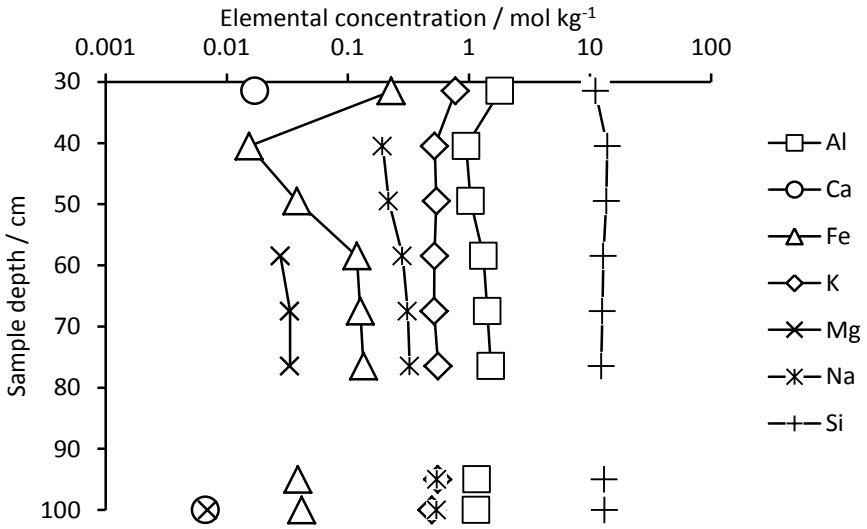

Fig. 4. The elemental chemistry of the bulk soil and bedrock normalised to 100 % at the a) DM02 and b) GD02 sites as determined by XRFS as a function of depth. Data plotted at 95 cm are for the altered bedrock and at 100 cm for the unaltered bedrock. These data are available in tabular form in the Supplementary Material.

1018 a.

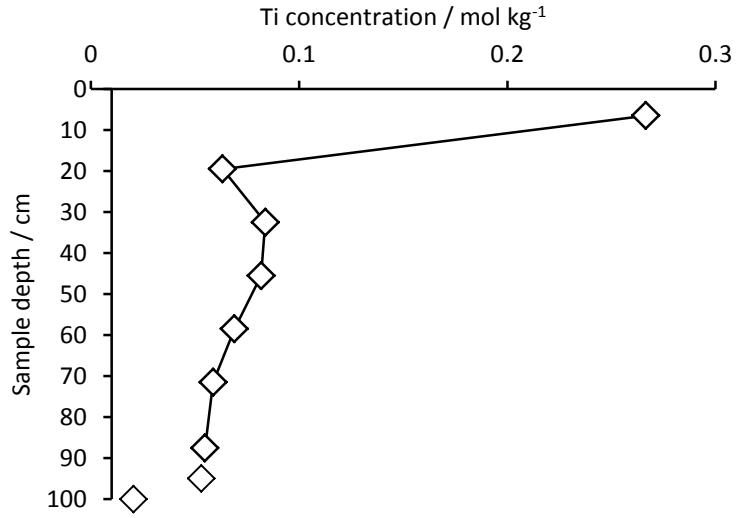

1019

1020 b.

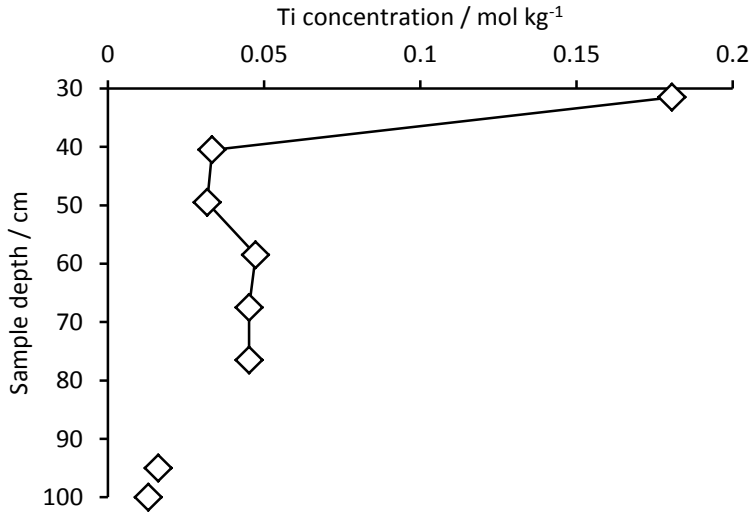

1021

1022

1023 **Fig. 5.** Ti concentrations of the bulk soil and bedrock normalised to 100 % at the a) DM02
1024 and b) GD02 sites as determined by XRFS as a function of depth. Data plotted at 95 cm are
1025 for the altered bedrock and at 100 cm for the unaltered bedrock.

1026 a.

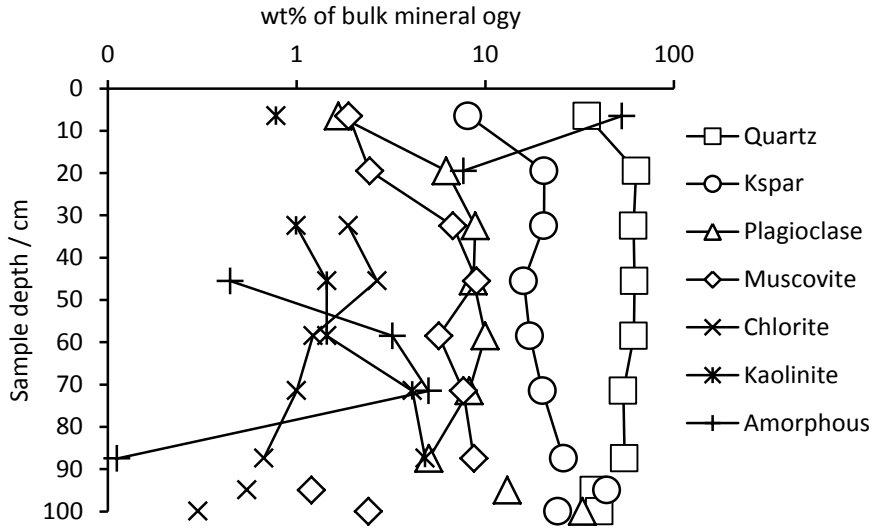

1027

1028 b.

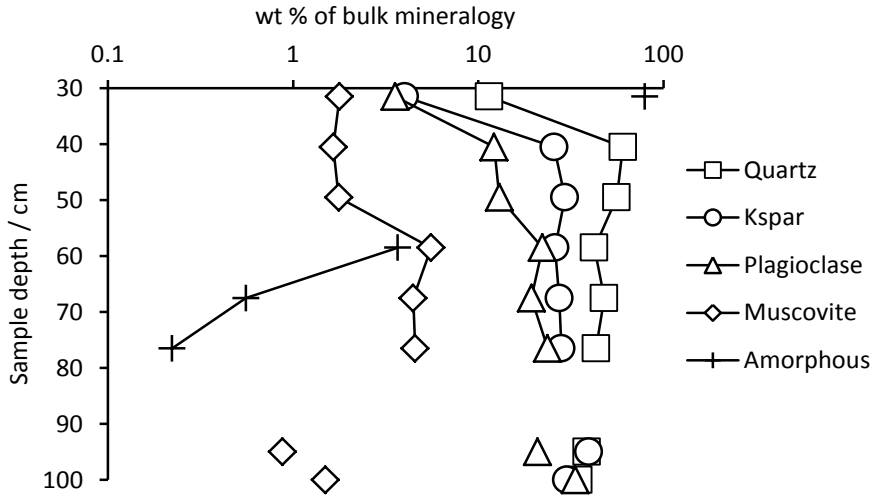

1029

1030 **Fig. 6.** Variation of mineralogy with depth for the a) DM02 and b) GD02 soil profiles and
1031 bedrock. Organic matter was removed from the samples by oxidation prior to analysis. Data
1032 plotted at 95 cm are for the altered bedrock and at 100 cm for the unaltered bedrock.

1033

a.

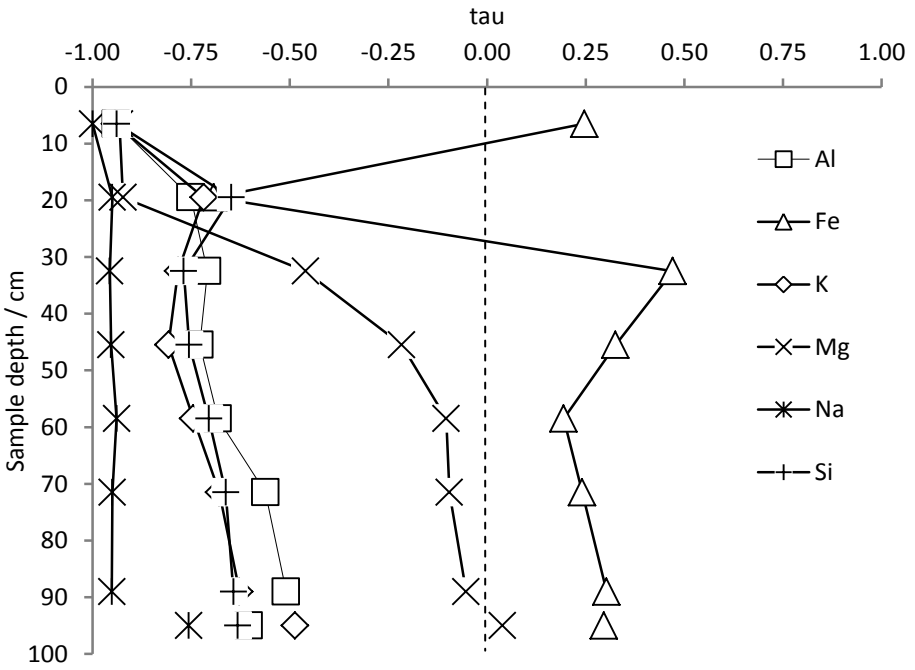

b.

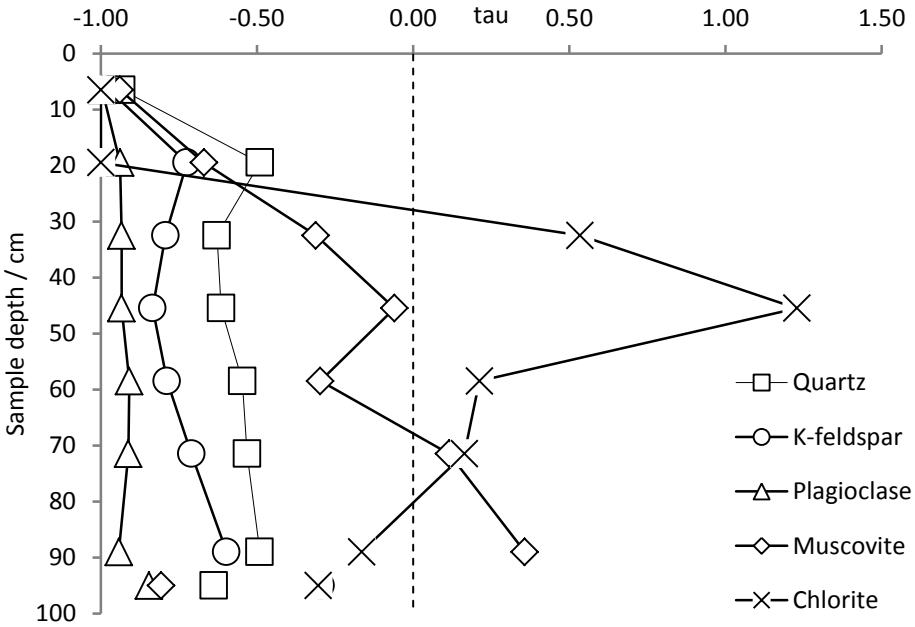

Fig. 7. The a) element and b) mineral phase τ plots for the DM02 soil profile. Data plotted at 95 cm are for the altered bedrock.

a.

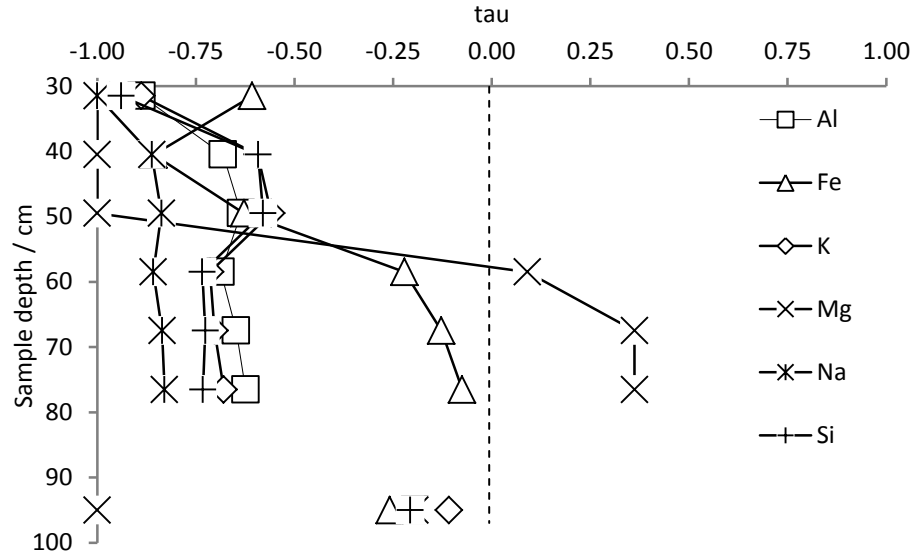

b

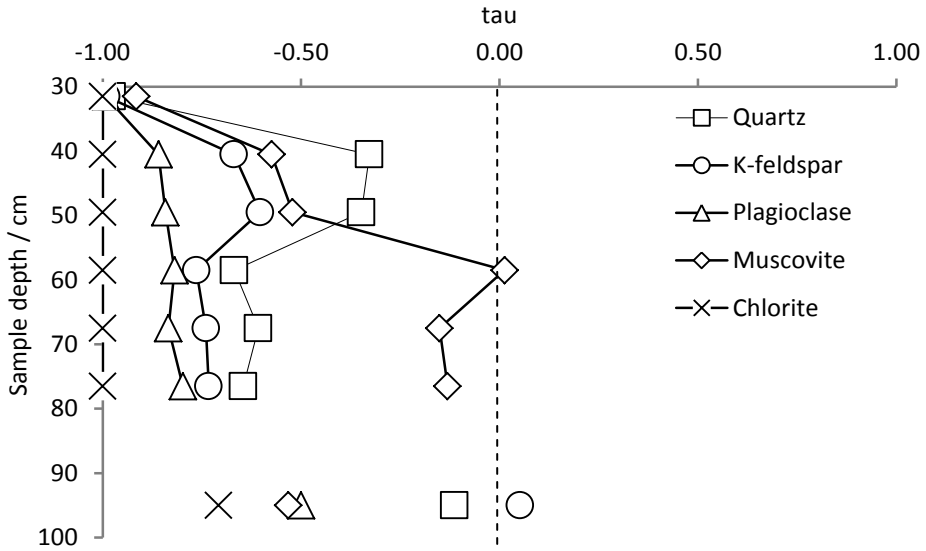

Fig. 8. The a) element and b) mineral phase τ plots for the GD02 soil profile. Data plotted at 95 cm are for the altered bedrock.

a.

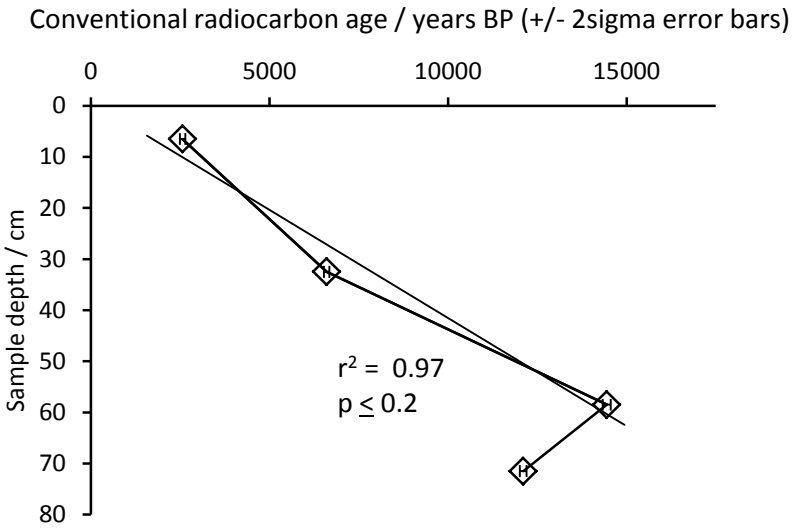

b.

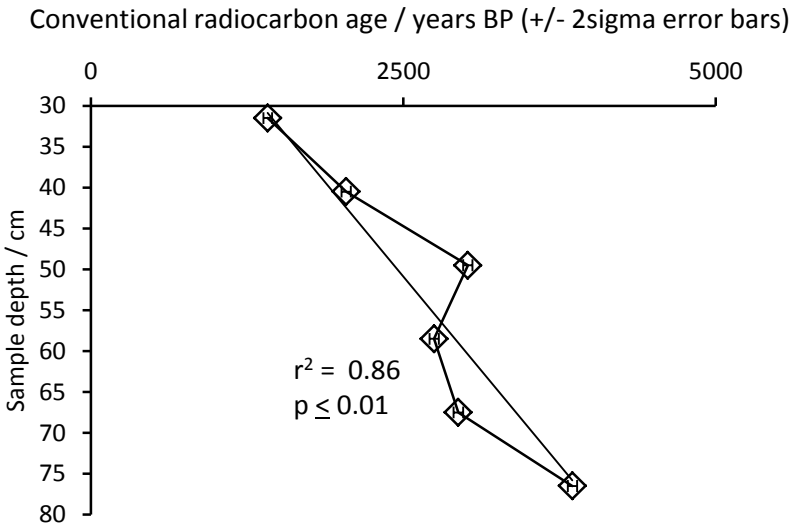

Fig. 9. Radiocarbon age of bulk soil humin fraction against sample depth in the a) DM02 and b) GD02 soil profiles. Weighted linear regression trend lines used 3 and 6 data points in the DM02 and GD02 soil profiles, respectively.

a.

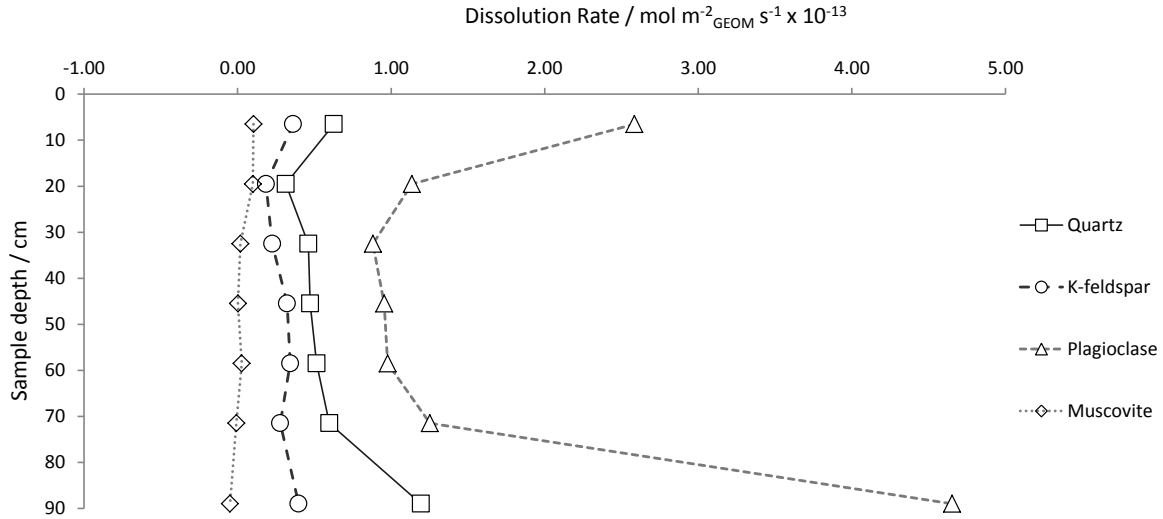

b.

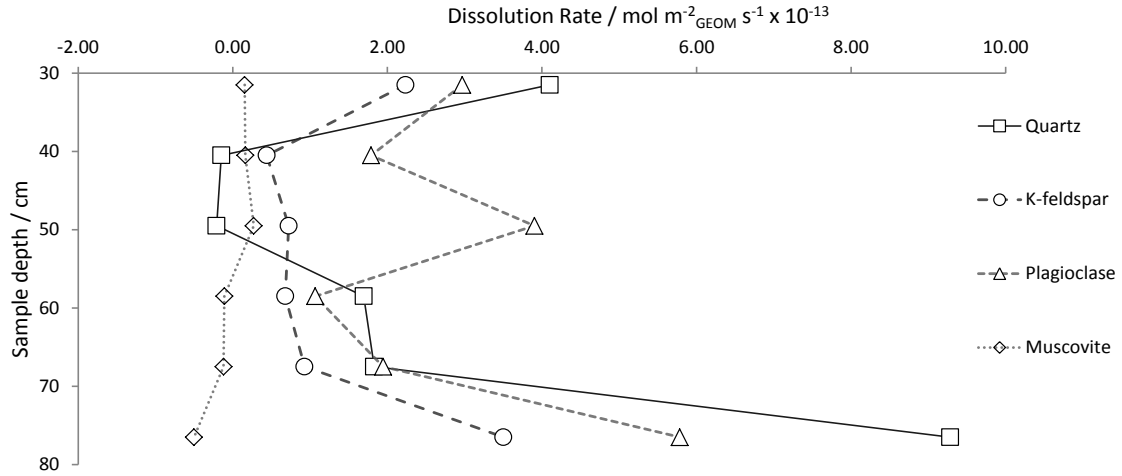

Fig. 10. The variation of the calculated mineral dissolution rates normalised to geometric surface area with sample depth in the a) DM02 and b) GD02 soil profiles. These data are available in tabular form in the Supplementary Material.

a.

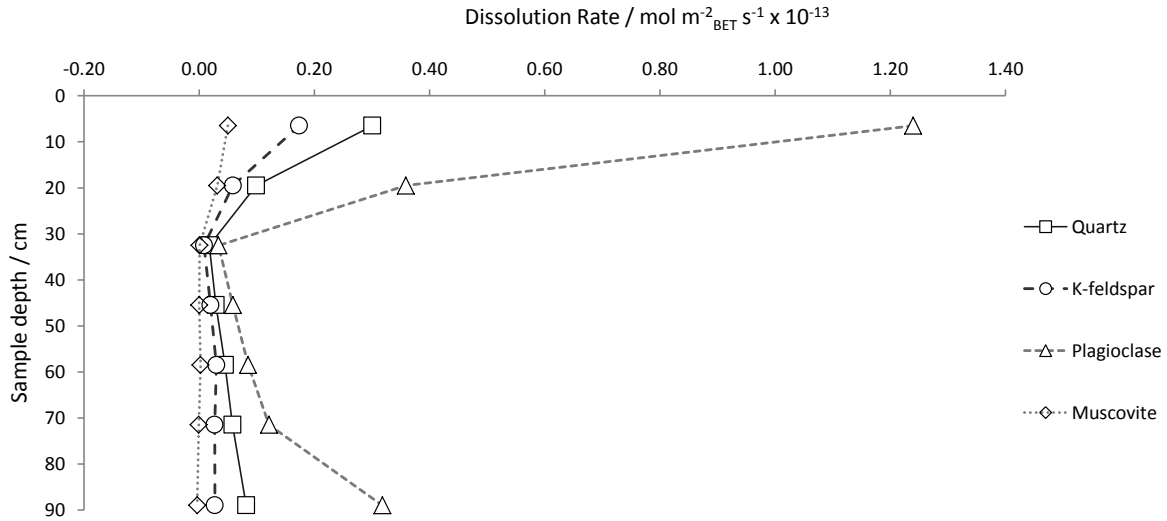

b.

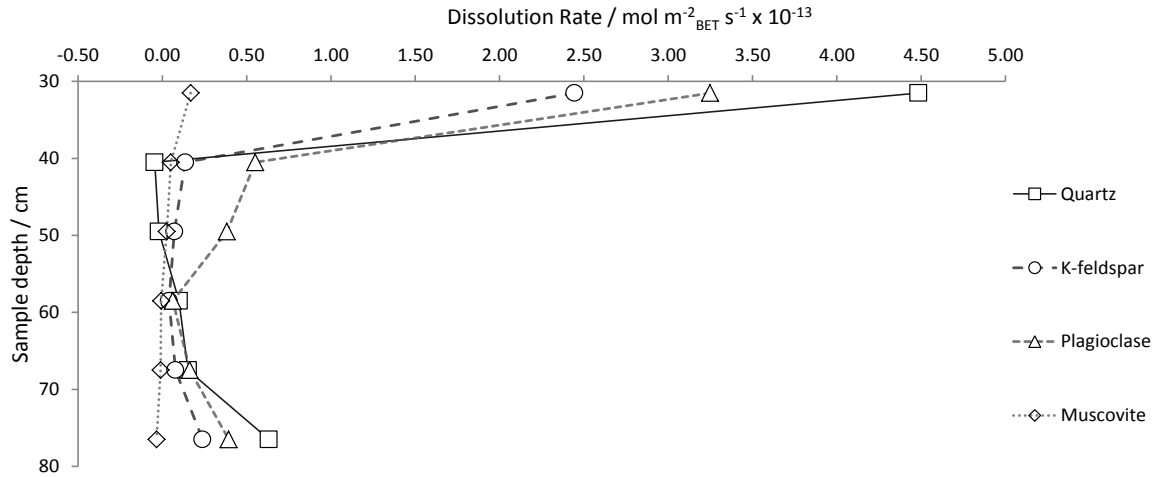

Fig. 11. The variation of the calculated mineral dissolution rates normalised to BET surface area with sample depth in the a) DM02 and b) GD02 soil profiles. These data are available in tabular form in the Supplementary Material.

a

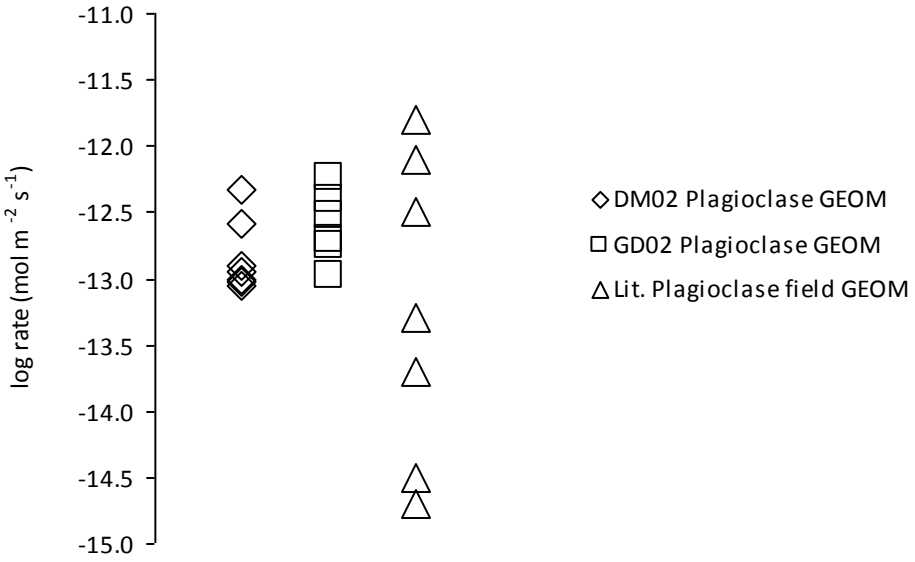

b

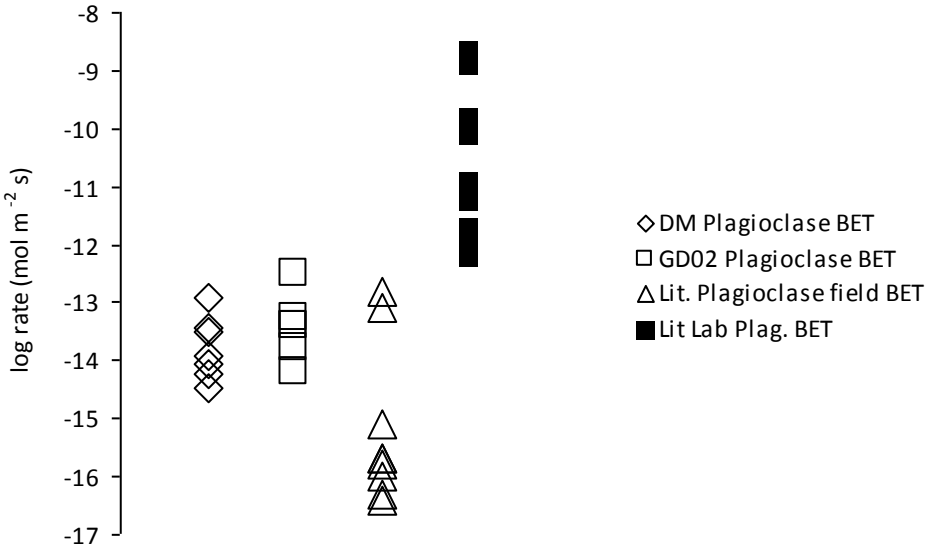

Fig. 12. A comparison of the plagioclase dissolution rates determined in this study and those reported in the literature. Rates are normalised to a) geometric and b) BET surface area. Literature field rates are taken from Table 2 in White (2009), whereas literature laboratory rates for intermediate plagioclases at 22-25 ºC and 3.5<pH<4.5 were taken from Casey et al., (1991), Welch and Ullmann (1993), Oxburgh et al. (1994), and Stillings et al. (1996). Note that much of the literature data were available as either BET or geometric surface area normalized rates, so do not appear in both plots.

1097 a

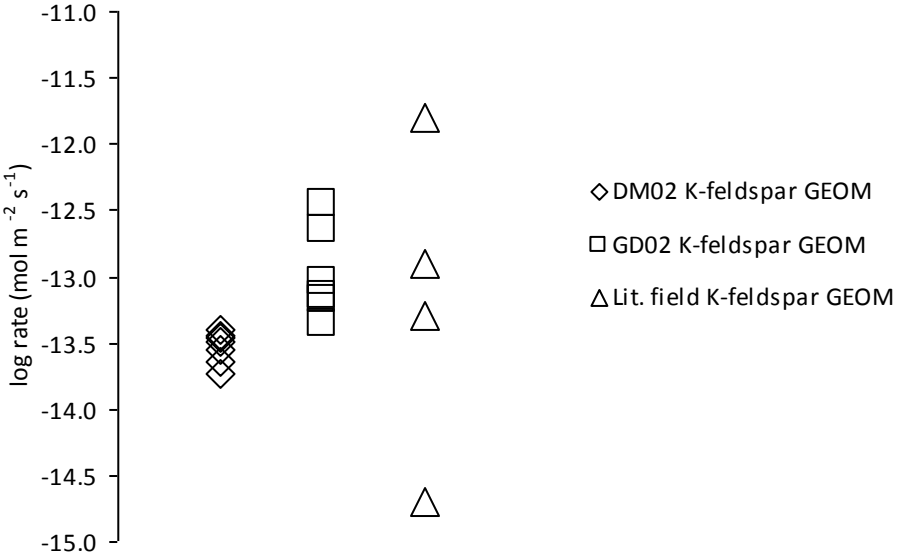

1098
1099
1100
1101 b

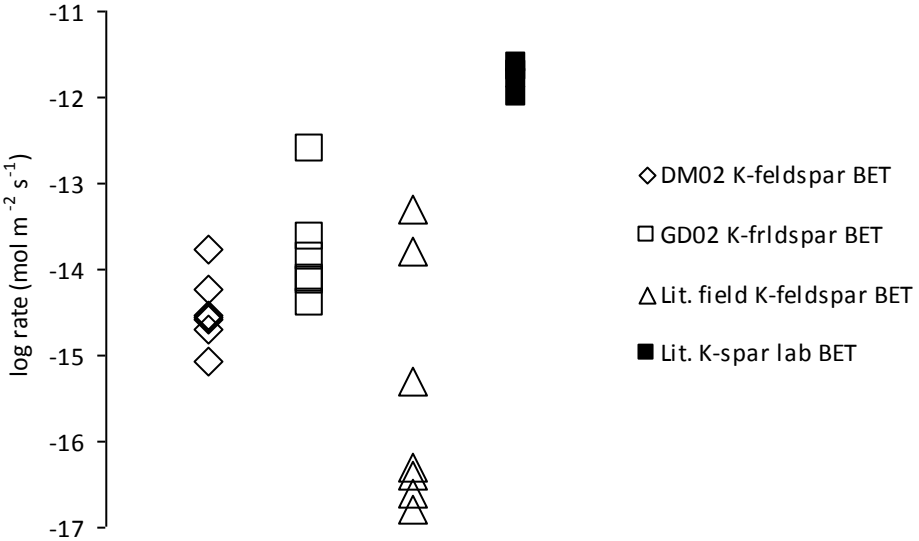

1102
1103

c.

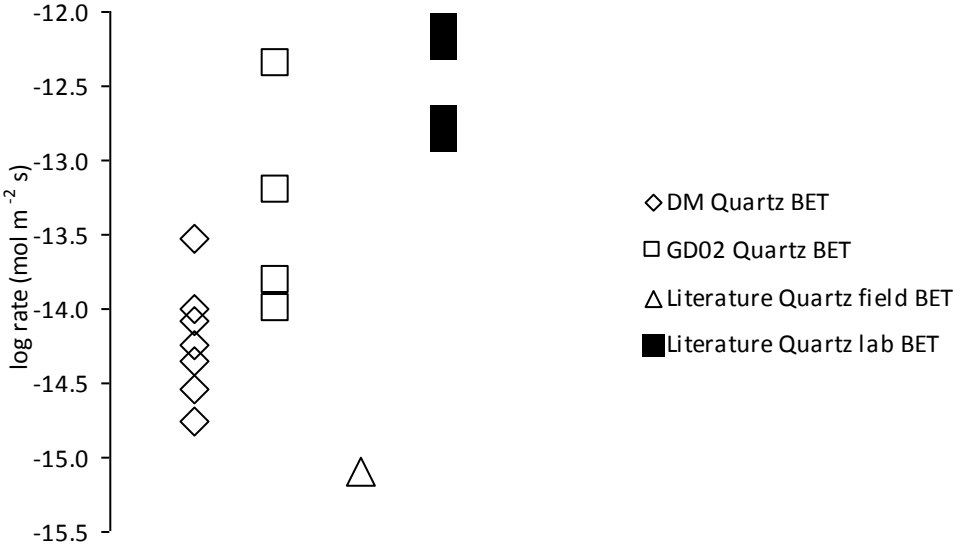

Fig. 13. A comparison of the rates determined in this study and those reported in the literature. Rates are normalised to a) geometric surface area normalized K-feldspar rates, b) BET surface area normalized K-feldspar rates, and c) BET surface area normalized quartz rates. Literature 'field' rates are taken from Table 2 in White (2009), whereas literature laboratory rates for temperatures from 22 to 25 °C and 3.5<pH<4.5 were taken from McCelland (1950), Wollast (1967), Manley and Evans (1986), and Schweda (1989) for K-feldspar, and Brady and Walther (1990), Sverdrup (1990), and Dove (1994) for quartz. Note that much of the literature data were available as either BET or geometric surface area normalized rates, so do not appear in both plots.

Supplementary material

Table S1. Compositional and physical data relating to profile DM02

Depth / cm	Mid point / cm	%OM	pH	A_{BET} / $m^2\ g^{-1}$	A_{GEOM} / $m^2\ g^{-1}$	^{14}C age	2σ
0 - 13	6.5	75	3.59	0.92	0.44	2565	74
13 - 26	19.5	14	3.86	0.92	0.29		
26 - 39	32.5	9	4.00	8.06	0.31	6602	77
39 - 52	45.5	5	4.13	5.65	0.35		
52 - 65	58.5	4	4.24	4.11	0.36	14445	113
65 - 78	71.5	4	4.36	4.71	0.46	12105	93
78 - 110	89	3	4.45	5.57	0.38		

Depth / cm	mol kg^{-1} Al	Ca	Fe	K	Mg	Mn	Na	P	Si	Ti
0 - 13	0.944	0.486	0.997	0.371	0.042	0.012	0.000	0.270	10.320	0.267
13 - 26	0.931	0.000	0.058	0.433	0.011	0.003	0.082	0.008	14.031	0.063
26 - 39	1.443	0.000	0.370	0.441	0.105	0.004	0.094	0.010	12.211	0.084
39 - 52	1.315	0.000	0.325	0.383	0.149	0.004	0.099	0.006	12.617	0.082
52 - 65	1.296	0.000	0.247	0.427	0.144	0.006	0.108	0.004	12.801	0.069
65 - 78	1.522	0.000	0.219	0.458	0.124	0.006	0.076	0.004	12.504	0.059
78 - 110	1.591	0.000	0.214	0.495	0.121	0.007	0.069	0.005	12.351	0.055
Altered rock	1.244	0.092	0.206	0.661	0.128	0.001	0.334	0.001	12.302	0.053
Bedrock	1.215	0.055	0.062	0.499	0.048	0.004	0.531	0.009	12.951	0.021

Depth / cm	wt % Quartz	Kspar	Plag	Muscovite	Chlorite	Kaolinite	Amorphous	Biotite
0 - 13	35	8	2	2	0	1	53	0
13 - 26	63	21	6	2	0	0	8	0
26 - 39	61	20	9	7	2	1	0	0
39 - 52	62	16	9	9	3	1	0	0
52 - 65	61	17	10	6	1	1	3	0
65 - 78	54	20	8	8	1	4	5	0
78 - 110	55	26	5	9	1	5	0	0
Altered rock	38	44	13	1	1	0	0	3
Bedrock	40	24	33	2	0	0	0	0

Kspar = potassium feldspar, Plag = plagioclase, Haem = haematite

1123 Table S2. Compositional and physical data relating to profile GD02

Depth / cm	Mid point / cm	%OM	pH	A_{BET} / m^2 g^{-1}	A_{GEOM} / m^2 g^{-1}	^{14}C age	2σ
27 - 36	31.5	89	3.32	0.35	0.38	1414	35
36 - 45	40.5	8	3.63	0.57	0.18	2042	37
45 - 54	49.5	4	3.84	0.96	0.09	3016	37
54 - 63	58.5	4	4.09	4.61	0.27	2745	37
63 - 72	67.5	4	4.16	3.50	0.29	2939	38
72 - 81	76.5	5	4.19	3.26	0.22	3852	38

Depth /	mol kg^{-1}									
Cm	Al	Ca	Fe	K	Mg	Mn	Na	P	Si	Ti
27 - 36	1.811	0.017	0.229	0.776	0.000	0.014	0.000	0.149	11.121	0.181
36 - 45	0.950	0.000	0.015	0.522	0.000	0.002	0.194	0.000	13.925	0.033
45 - 54	1.036	0.000	0.038	0.539	0.000	0.001	0.218	0.000	13.670	0.032
54 - 63	1.323	0.000	0.119	0.520	0.028	0.006	0.283	0.001	12.883	0.047
63 - 72	1.422	0.000	0.127	0.517	0.033	0.006	0.313	0.004	12.660	0.045
72 - 81	1.520	0.000	0.135	0.557	0.033	0.006	0.325	0.005	12.394	0.045
Altered rock	1.161	0.000	0.039	0.553	0.000	0.001	0.548	0.001	13.111	0.016
Bedrock	1.153	0.007	0.042	0.496	0.007	0.001	0.544	0.002	13.203	0.013

Depth /	wt %				
cm	Quartz	Kspar	Plagioclase	Muscovite	Amorphous
27 - 36	11	4	4	2	79
36 - 45	60	26	12	2	0
45 - 54	56	29	13	2	0
54 - 63	42	26	22	6	4
63 - 72	48	27	19	4	1
72 - 81	43	28	24	5	0
Altered rock	39	39	21	1	0
Bedrock	35	30	33	1	0

1124 Kspar = potassium feldspar
1125

Table S3. Mineral dissolution rates normalised to geometric surface area / mol m^{-2} s^{-1}

DM02					
Depth / cm	Mid point / cm	Quartz	Plagioclase	K-feldspar	Muscovite
0 – 13	6.5	6.27E-14	2.58E-13	3.62E-14	1.04E-14
13 – 26	19.5	3.14E-14	1.14E-13	1.85E-14	9.97E-15
26 – 39	32.5	4.61E-14	8.81E-14	2.26E-14	1.86E-15
39 – 52	45.5	4.73E-14	9.55E-14	3.22E-14	2.84E-16
52 – 65	58.5	5.15E-14	9.77E-14	3.43E-14	2.72E-15
65 – 78	71.5	5.98E-14	1.25E-13	2.78E-14	-8.21E-16
78 - 110	89	1.19E-13	4.65E-13	3.97E-14	-4.91E-15

GD02					
Depth / cm	Mid point / cm	Quartz	Plagioclase	K-feldspar	Muscovite
27 - 36	31.5	4.10E-13	2.97E-13	2.24E-13	1.54E-14
36 - 45	40.5	-1.48E-14	1.79E-13	4.40E-14	1.63E-14
45 - 54	49.5	-2.10E-14	3.90E-13	7.24E-14	2.70E-14
54 - 63	58.5	1.69E-13	1.07E-13	6.79E-14	-1.09E-14
63 - 72	67.5	1.83E-13	1.94E-13	9.29E-14	-1.19E-14
72 - 81	76.5	9.28E-13	5.78E-13	3.50E-13	-5.02E-14

Table S4. Mineral dissolution rates normalised to BET surface area / mol m^{-2} s^{-1}

DM02					
Depth / cm	Mid point / cm	Quartz	Plagioclase	K-feldspar	Muscovite
0 – 13	6.5	3.01E-14	1.24E-13	1.74E-14	4.98E-15
13 – 26	19.5	9.91E-15	3.59E-14	5.85E-15	3.15E-15
26 – 39	32.5	1.75E-15	3.35E-15	8.57E-16	7.08E-17
39 – 52	45.5	2.90E-15	5.86E-15	1.98E-15	1.74E-17
52 – 65	58.5	4.49E-15	8.51E-15	2.99E-15	2.37E-16
65 – 78	71.5	5.79E-15	1.21E-14	2.69E-15	-7.95E-17
78 - 110	89	8.17E-15	3.18E-14	2.72E-15	-3.36E-16

GD02					
Depth / cm	Mid point / cm	Quartz	Plagioclase	K-feldspar	Muscovite
27 - 36	31.5	4.48E-13	3.25E-13	2.44E-13	1.68E-14
36 - 45	40.5	-4.57E-15	5.52E-14	1.36E-14	5.01E-15
45 - 54	49.5	-2.06E-15	3.83E-14	7.10E-15	2.65E-15
54 - 63	58.5	9.89E-15	6.23E-15	3.96E-15	-6.34E-16
63 - 72	67.5	1.53E-14	1.63E-14	7.76E-15	-9.97E-16
72 - 81	76.5	6.32E-14	3.94E-14	2.38E-14	-3.41E-15